

TRANSIENT HYDRAULIC SIMULATION: BREACHED EARTH DAMS

by

DANNY LEE FREAD, 1938-

A DISSERTATION

Presented to the Faculty of the Graduate School of the

UNIVERSITY OF MISSOURI-ROLLA

In Partial Fulfillment of the Requirements for the Degree

DOCTOR OF PHILOSOPHY

in

CIVIL ENGINEERING

1971

Steve Harbaugh
Advisor

Joseph W. House

C. Y. Ho

Ralph E. Lee

Wesley S. Anderson

W. H. Hill

PUBLICATION THESIS OPTION

This thesis has been prepared in the style utilized by the Journal of the Hydraulics Division, American Society of Civil Engineers. Pages 1-65 will be presented for publication in that journal. The Vita has been added for purposes normal to thesis writing. Additional experimental data and the simulation computer program are contained within reference (12), "Simulation Program for the Transient Hydraulics Produced by Gradually Breached Dams," *Hydraulic Series Bulletin*, Civil Engineering Studies, University of Missouri-Rolla, Rolla, Missouri, May 1971.

TRANSIENT HYDRAULIC SIMULATION: BREACHED EARTH DAMS

By Danny L. Fread¹, M. ASCE

KEY WORDS: breach; computer; earth dams; hydraulics; method of characteristics; numerical model; reservoirs; simulation; St. Venant equations; transient open-channel flow.

Abstract: A conceptual method to alleviate flood damages due to overtopping failures of small earthfill dams is the incorporation of a relatively thin erosion retarding layer within the dam. This paper investigates the reduction in the reservoir release due to the hypothetical erosion retarding layer. In addition, the paper provides a method for the determination of an optimal location of the layer so as to minimize the maximum possible reservoir release due to a gradually breached earth dam. The transient reservoir flow is simulated by a numerical model, based upon the solution of the one-dimensional St. Venant unsteady open-channel flow equations. These equations are solved by the method of characteristics, with appropriate boundary conditions incorporated into the solution procedure. The numerical simulation model is used to determine the reduction in reservoir release due to a single retarding layer and its optimal location for a wide range of pertinent geometric, hydraulic and dynamic parameters. The sensitivity of the results to variations in the above parameters is discussed.

¹Research Assistant, Civil Engineering Department, University of Missouri-Rolla, Rolla, Missouri 65401.

TABLE OF CONTENTS

	Page
ABSTRACT.....	ii
LIST OF FIGURES.....	v
LIST OF TABLES.....	vii
INTRODUCTION.....	1
THEORY.....	2
St. Venant Differential Equations.....	2
Reservoir Geometry.....	6
Breach Geometry and Dynamics.....	11
NUMERICAL SIMULATION MODEL.....	12
Dimensional and Geometrical Considerations.....	12
Initial Conditions.....	14
Steady State Parameters.....	16
Numerical Solution of St. Venant Equations.....	18
Characteristic Equations.....	19
Upstream Boundary.....	24
Interior Points.....	26
Downstream Boundary.....	26
Optimization of Retarding Layer Location.....	29
Modifications to Model.....	30
EXPERIMENTAL SIMULATION MODEL.....	33
NUMERICAL RESULTS.....	35
Comparison with Experimental Results.....	35
Retarding Layer: Optimal Location and Reduction in Outflow.....	38

	Page
Sensitivity to Variations in Fixed Parameters.....	56
Computation Time.....	56
SUMMARY AND CONCLUSIONS.....	58
ACKNOWLEDGEMENT.....	60
APPENDIX I. - REFERENCES.....	60
APPENDIX II. - NOTATION.....	62
VITA.....	66

LIST OF FIGURES

Figure	Page
1. Elementary Channel Reach.....	5
2. Reservoir Cross Section With Earthfill Dam.....	8
3. Idealized Reservoir.....	10
4. $x^* - t^*$ Plane With Characteristic Network.....	23
5. Typical Variation Of The Percent Reduction (QR) In The Maximum Possible Reservoir Release With The Location (η_{lt}^*) Of The Erosion Retarding Layer.....	32
6. Stage and Discharge Hydrographs Of Experimental Run No. 5.....	37
7. Relationship Between QR_{max} And η_{lt0p}^* For Various Values Of λ^* And $L = 10,000$ ft., $\tau = 10$, $\lambda_c = 0.1$ fps.....	40
8. Relationship Between QR_{max} And η_{lt0p}^* For Various Values Of λ^* And $L = 10,000$ ft., $\tau = 10$, $\lambda_c = 0.01$ fps.....	42
9. Relationship Between QR_{max} And η_{lt0p}^* For Various Values Of λ^* And $L = 10,000$ ft., $\tau = 10$, $\lambda_c = 0.005$ fps.....	44
10. Relationship Between QR_{max} And η_{lt0p}^* For Various Values Of λ^* And $L = 2,000$ ft., $\tau = 4$, $\lambda_c = 0.1$ fps.....	46
11. Relationship Between QR_{max} And η_{lt0p}^* For Various Values Of λ^* And $L = 2,000$ ft., $\tau = 4$, $\lambda_c = 0.01$ fps.....	48
12. Relationship Between QR_{max} And η_{lt0p}^* For Various Values Of λ^* And $L = 2,000$ ft., $\tau = 4$, $\lambda_c = 0.005$ fps.....	50

13. Relationship Between QR_{max} And η^* For Various Values
 Of λ^* And $L = 10,000$ ft., $\tau = 10$, $\lambda_m = 0.1$ fps, $y_{dm} = 0.97$
 ($\eta = 50$ ft.), $y_{dm} = 0.91$ ($\eta = 100$ ft.) And λ Is An Exponential
 Function..... 53
14. Relationship Between QR_{max} And η^* For Various Values
 Of λ^* and $L = 10,000$ ft., $\tau = 10$, $\lambda_m = 0.01$ fps, $y_{dm} = 0.90$
 ($\eta = 50$ ft.), $y_{dm} = 0.58$ ($\eta = 100$ ft.) And λ Is An Exponential
 Function..... 55

LIST OF TABLES

Table	Page
1. Sensitivity of η_{ltOp}^* And QR_{max} To Variations In K_1 , η_{ld}^* , η_{sp}^* , z , τ , C_v And n For $L = 10,000$ ft., $\tau = 10$, $\lambda_c = 0.01$ fps.....	57

INTRODUCTION

Numerous small homogeneous earthfill dams, up to approximately 100 ft. in height, have failed or are subject to possible failure from over-topping because of inadequate spillways (20, 31).² Such failures may cause considerable property damage and even the loss of life. Inadequate spillways prevalent on many dams are generally due to the lack of engineering consultation during design and construction; however, even with engineering advice, incomplete or unavailable hydrologic data may result in the spillway being designed for less than the critical storm, resulting in the eventual failure or breach of the structure.

A conceptual method of alleviating downstream damages from breached earth dams is to provide a relatively thin erosion retarding layer at an optimal elevation within the dam. Thus, in the event of an over-topping of the dam, the resulting breach would not develop continuously but rather be delayed by the hypothetical erosion retarding layer. Such a controlled breach would produce two distinct flood waves of a reduced amplitude compared to the single flood wave produced by a breach of an earth dam without a retarding layer. Consequently, a reduction in downstream damages would be obtained.

In this paper, the hydraulic characteristics of transient reservoir flow resulting from gradually breached earthfill dams are investigated in order to ascertain the reduction of the flood wave peak due

²Numerals in parentheses refer to corresponding items in Appendix I. -
References

to a retarding layer. This reduced flood wave peak discharge is shown to be directly attributable to the retarding layer's effect in reducing the reservoir outflow.

Basic assumptions concerning the geometric and dynamic aspects of the phenomenon are made in order to develop a generalized numerical simulation model of the transient reservoir flow due to a breached dam. An experimental model is used to verify the numerical model. The numerical model is used to determine the expected reduction in outflow due to a single retarding layer for several pertinent geometric, dynamic, and hydraulic parameters. Also, the elevation of the retarding layer is optimized such that the maximum possible outflow from a gradually breached dam is minimized.

THEORY

St. Venant Differential Equations. - The basis for formulating a numerical simulation model of the transient reservoir flow due to a gradually breached dam is the premise that such a phenomenon is well-approximated by the one-dimensional differential equations of gradually varied, unsteady channel flow. These equations are attributed to A.J.C. Barre' de Saint-Venant and are known as the "St. Venant equations". They are derived in several references (5,11,15,25,27) and are simply stated herein as

$$\frac{\partial y}{\partial t} + D \frac{\partial v}{\partial x} + v \frac{\partial y}{\partial x} = 0 \dots \dots \dots (1)$$

$$\frac{\partial v}{\partial t} + v \frac{\partial v}{\partial x} + g \frac{\partial y}{\partial x} + g(S_f - S_o) = 0 \dots \dots \dots (2)$$

in which y = the depth of flow in the channel, v = the average velocity across a section of channel, D = the hydraulic mean depth which is equivalent to A/T , T = the width of the free water surface, A = the cross-sectional area, g = the acceleration due to gravity, x = the distance along the channel, and t = the time. In this paper, the channel (reservoir) is prismatic, and S_o = the slope of the reservoir bottom which is small and is approximated by $\sin \theta$, where θ is the angle of inclination of the reservoir bottom with a horizontal datum line. Hydrostatic conditions exist throughout the flowing fluid, and the resistance to flow due to the shear force at the wetted perimeter P is accounted for by use of Manning's equation for steady uniform flow. Thus, the friction slope S_f , which is the slope of the energy grade line, can be approximated by

$$S_f = \frac{n^2 |v| v}{2.2 R^{4/3}} \dots \dots \dots (3)$$

in which n = the Manning coefficient, and the hydraulic radius $R = A/P$. Hence, the St. Venant equations, which are quasi-linear hyperbolic partial differential equations, describe the transient flow within the element of water that is bounded by two vertical cross sections shown in Fig. 1. Eq. 1 is known as the "equation of continuity" and mathematically expresses the Law of Conservation of Mass of the incompressible fluid within the element. Eq. 2, which is derived from Newton's Second Law of Motion, is known as the "equation of motion" and expresses the Law of Conservation of Momentum of the fluid within the element.

The initial condition of the flow within the reservoir, i.e. the depths and velocities, must be known in order that solutions to the

FIGURE 1. ELEMENTARY CHANNEL REACH

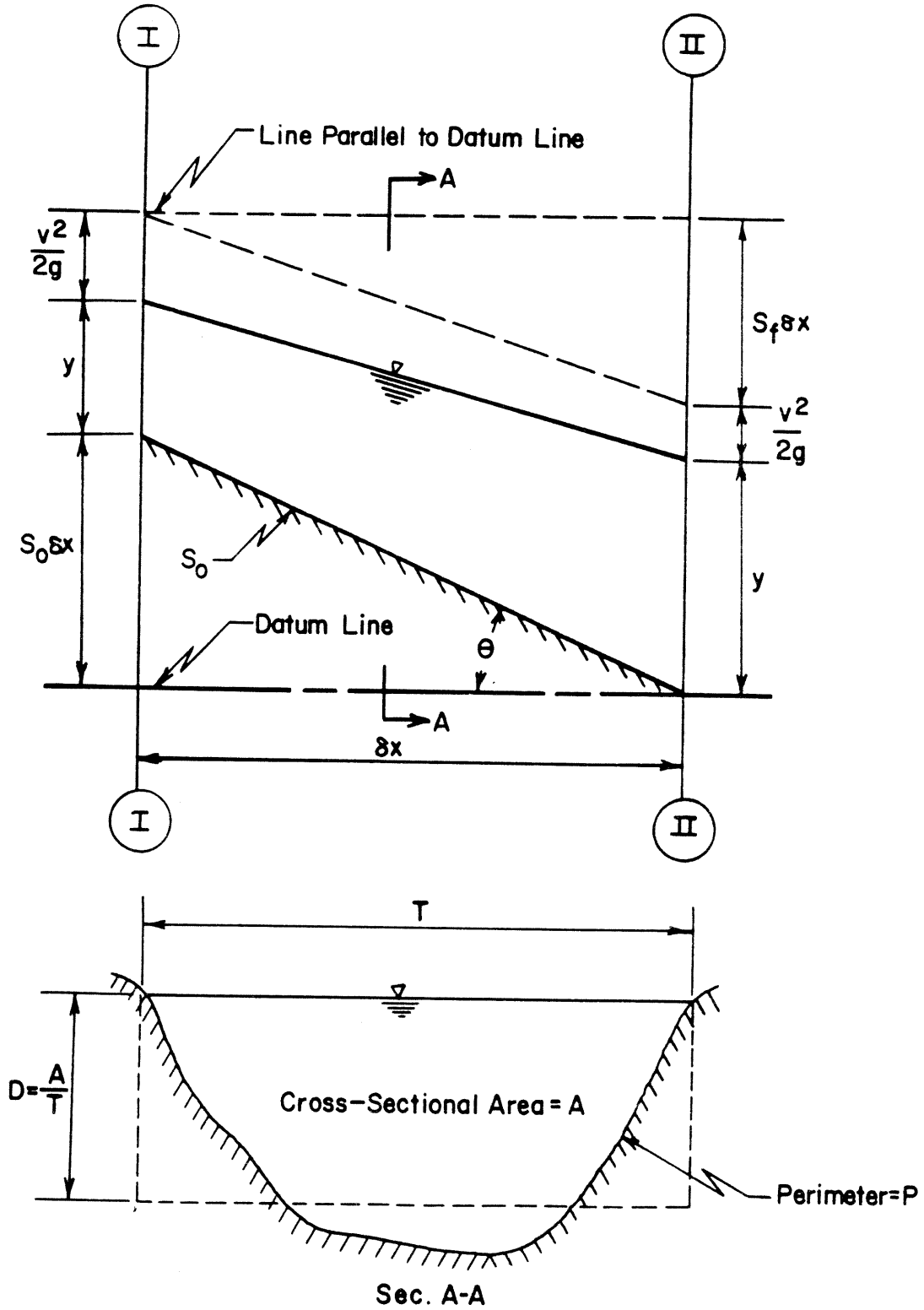


FIGURE 1.

St. Venant equations may be obtained. The initial condition of the flow may be steady gradually varied, unsteady gradually varied, or steady uniform flow, etc.

Boundary conditions at the upstream and downstream extremities of the reservoir are essential to the solution of the St. Venant equations. A boundary condition is a known relationship between any two of the variables v , y , t and the flow rate Q throughout the time that solutions to the equations are desired. The upstream boundary condition, used in this paper, is a known relationship between Q_u and t , i.e. $Q_u = Q_u(t)$. The downstream boundary is provided by a stage-discharge relationship, i.e. $Q_d = Q_d(y)$. The downstream boundary is located a short distance upstream of the breached dam at a section where the flow is well-approximated as one-dimensional and the surface drawdown due to the outflow through the spillway and breach is negligible.

Reservoir Geometry. - The reservoir cross section is assumed trapezoidal with side slopes of 1:vertical to z :horizontal, as shown in Fig. 2. Only the prismatic portion of the idealized reservoir shown in Fig. 3 is considered to contribute to the outflow released by a breached dam. The storage in the upper reaches of the reservoir provides little contribution to the outflow since accumulated sediment deposits soon reduce this storage to a negligible quantity. Thus, the upstream boundary is located at the upper end of the prismatic reservoir, a distance L from the downstream boundary.

The reservoir bottom slope, S_o , is constant and defined as

$$S_o = \frac{n}{L}, \dots\dots\dots(4)$$

FIGURE 2. RESERVOIR CROSS SECTION WITH EARTHFILL DAM

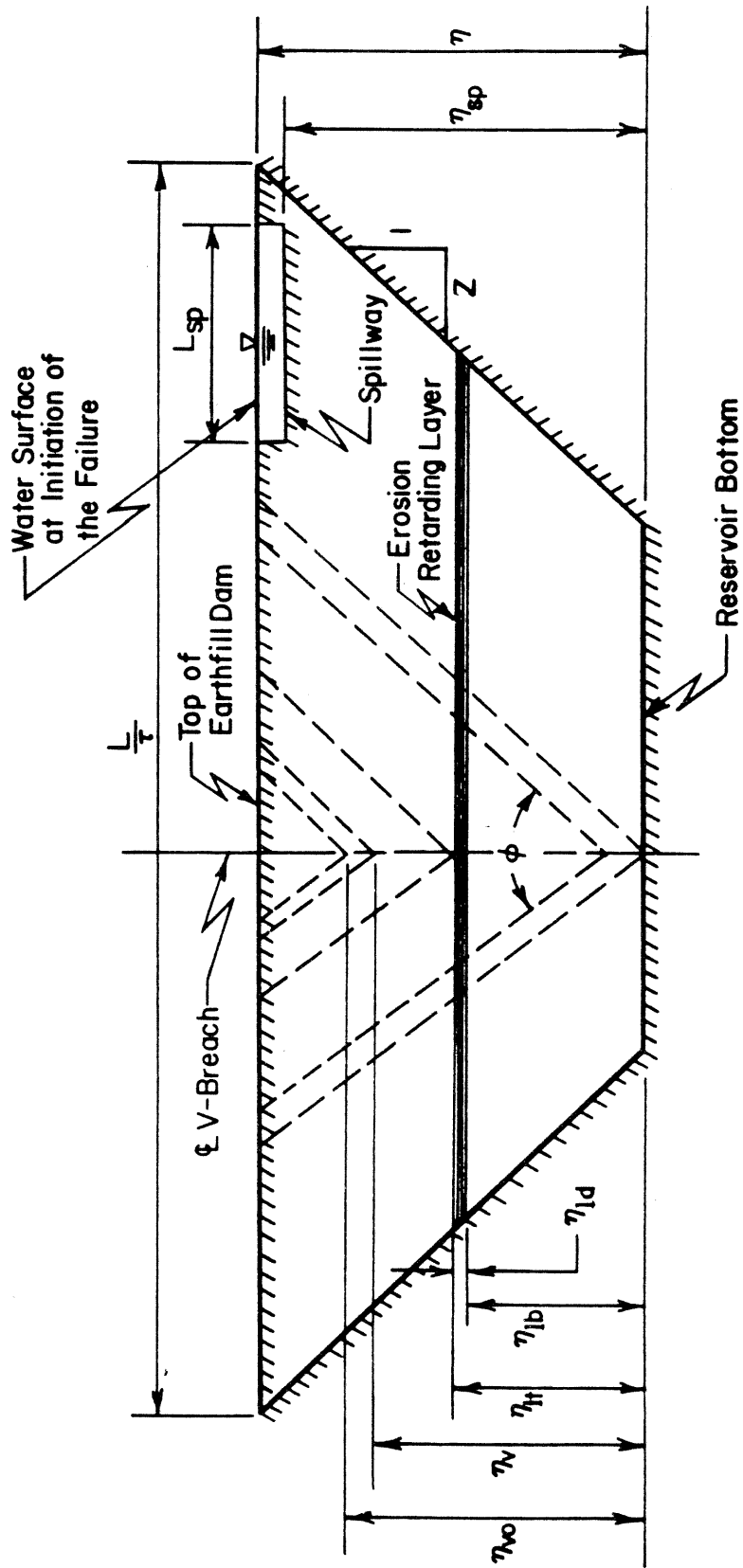


FIGURE 2.

FIGURE 3. IDEALIZED RESERVOIR

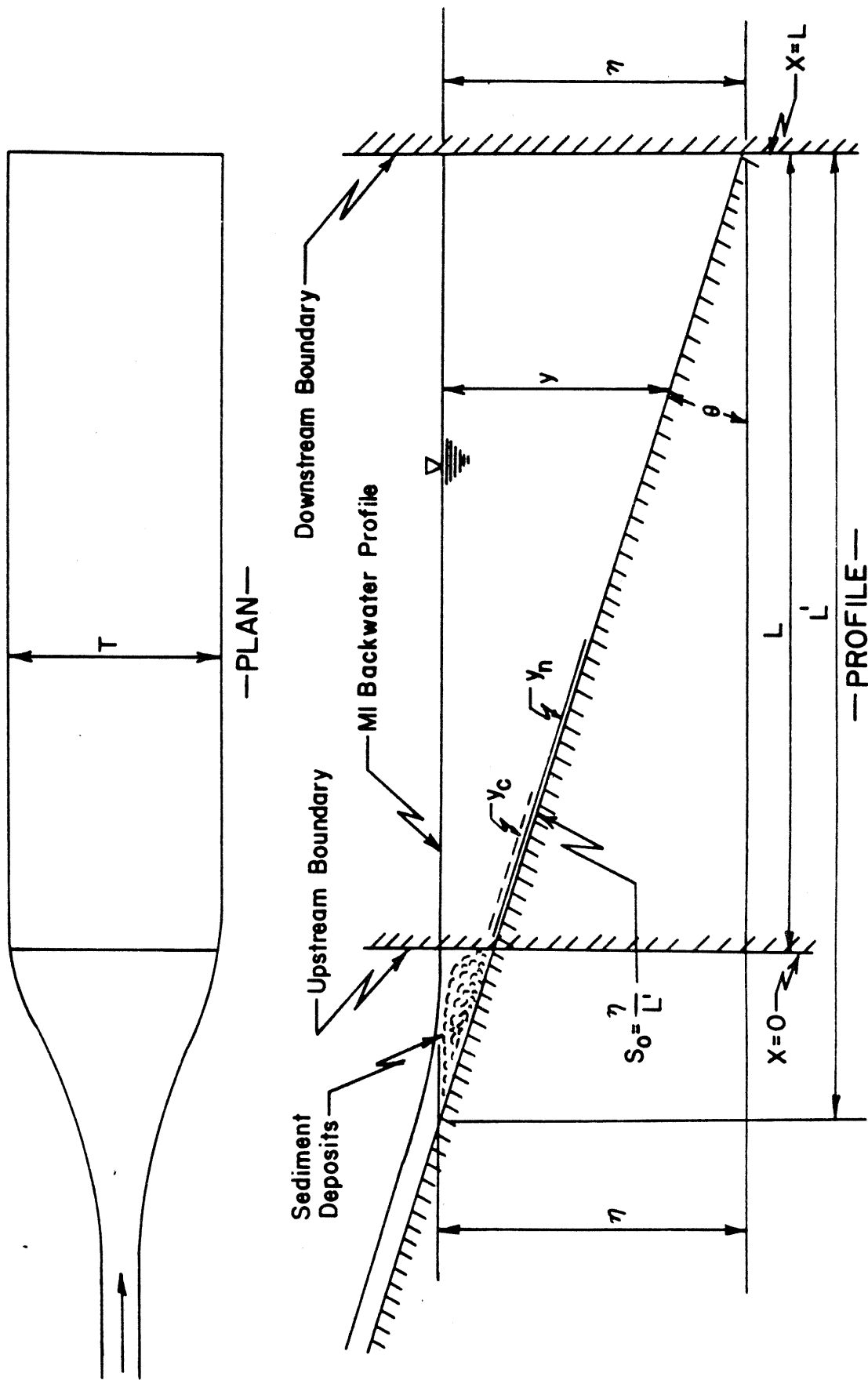


FIGURE 3.

where η is the height of the dam and L' is the distance from the downstream boundary to the intersection with the reservoir bottom of a horizontal line drawn from the top of the dam, as shown in Fig. 3.

In this investigation, L is defined as

$$L' = K_1 L \dots\dots\dots(5)$$

where K_1 is a constant.

Breach Geometry and Dynamics. - The breach is assumed to commence forming at the instant the maximum capacity Q_0 of the emergency and/or principal spillway is exceeded and the dam is over-topped. Referring to Fig. 2, the spillway is located at an elevation η_{sp} , and the breach is assumed to form as a "V" where the acute central angle ϕ of the "V-breach" remains constant throughout its formation. This breach geometry is assumed to approximate that caused by the over-topping of a homogeneous earthfill dam (31).

The breach forms at a rate denoted by λ , which has dimensions of fps, and is defined as the vertical distance traversed by the bottom-most point of the V-breach during an increment of time. Two basic types of failure rates, λ , are investigated herein. The first type is

$$\lambda = \lambda_c \dots\dots\dots(6)$$

where λ_c is constant for a particular interval of time during the failure or for a particular span of vertical distance within the dam; λ_c may be expressed as a step-function of either time or elevation. For the other type of failure rate, λ is assumed to be an exponential function of the head on the V-breach, where the head is defined as $(y_d - \eta_v)$.

Thus,

$$\lambda = \exp [K_e (y_d - \eta_v)] - 1 \dots \dots \dots (7)$$

where
$$K_e = \frac{\ln(1+\lambda_m)}{y_{dm}} \dots \dots \dots (8)$$

and y_d is the transient reservoir depth at the downstream boundary, η_v is the elevation of the bottom of the V-breach, and λ_m and y_{dm} are respectively the maximum failure rate and reservoir depth at the downstream boundary when $\eta_v = 0$. When the bottom point of the V-breach is in contact with the erosion retarding layer, the failure rate is significantly reduced to a value of λ/K_λ , where K_λ is a constant greater than unity. The top of the erosion retarding layer is denoted as η_{1t} , the bottom as η_{1b} , and the thickness as η_{1d} .

NUMERICAL SIMULATION MODEL

Dimensional and Geometrical Considerations. - The St. Venant equations are nondimensionalized herein by defining the following dimensionless variables

$$y^* = \frac{y}{\eta}, \quad v^* = \frac{v}{v_\eta}, \quad x^* = \frac{x}{L}, \quad t^* = \frac{t v_\eta}{L} \dots \dots \dots (9)$$

$$D^* = \frac{D}{D_\eta} = \frac{c_1 (c_1 y^{*2} - 2c_2 y^* + c_2^2)}{(c_1 - c_2)(c_1 - 2c_2 + 2c_2 y^*)} \dots \dots \dots (10)$$

$$R^* = \frac{R}{R_\eta} = \frac{(c_1 - 2c_2 + c_3)(c_1 y^{*2} - 2c_2 y^* + c_2^2)}{(c_1 - c_2)(c_1 - 2c_2 + c_3 y^*)} \dots \dots \dots (11)$$

in which $c_1 = \frac{L}{\tau}$, $c_2 = z\eta$, and $c_3 = 2\eta\sqrt{1+z^2} \dots \dots \dots (12)$

and τ is the ratio of the reservoir top width T to the reservoir length L . The η subscript indicates that the subscripted variable is evaluated

at the downstream boundary when $t = 0$, $\eta_v = \eta$. The $*$ superscript is used henceforth to denote a variable as being dimensionless.

Substitution of Eq. 3 along with the above dimensionless variables into Eqs. 1 and 2, taking care to properly express the partial derivatives, yields the following dimensionless form of the St. Venant equations

$$\frac{\partial y^*}{\partial t^*} + K_1 D^* \frac{\partial v^*}{\partial x^*} + v^* \frac{\partial y^*}{\partial x^*} = 0 \dots\dots\dots(13)$$

$$\frac{\partial v^*}{\partial t^*} + v^* \frac{\partial v^*}{\partial x^*} + K_2 \frac{\partial y^*}{\partial x^*} + \frac{K_3 |v^*| v^*}{R^{*4/3}} - K_4 = 0 \dots\dots\dots(14)$$

where $K_1 = \frac{(c_1 - c_2)}{c_1} \dots\dots\dots(15)$

$$K_2 = \frac{g\eta^3 (c_1 - c_2)^2}{Q_o^2} \dots\dots\dots(16)$$

$$K_3 = \frac{g\eta^2 L}{2.21\eta^{4/3}} \left[\frac{(c_1 - 2c_2 + c_3)}{(c_1 - c_2)} \right]^{4/3} \dots\dots\dots(17)$$

$$K_4 = \frac{gS_o L \eta^2 (c_1 - c_2)^2}{Q_o^2} \dots\dots\dots(18)$$

The following dimensionless variables are defined in order that the boundary conditions may be expressed in dimensionless form

$$\lambda^* = \frac{\lambda L}{Q_o} (c_1 - c_2), \quad Q_u^* = \frac{Q_u}{Q_o}, \quad Q_d^* = \frac{Q_d}{Q_o} \dots\dots\dots(19)$$

$$\eta_{sp}^* = \frac{\eta_{sp}}{\eta}, \quad \eta_v^* = \frac{\eta_v}{\eta}, \quad \eta_{lt}^* = \frac{\eta_{lt}}{\eta}, \quad \eta_{lb}^* = \frac{\eta_{lb}}{\eta},$$

$$\eta_{ld}^* = \frac{\eta_{ld}}{\eta} \dots\dots\dots(20)$$

The u and d subscripts refer to the upstream and downstream boundaries, respectively.

The above normalizing procedure allows y^* and η_v^* to take on values from unity to zero and v^* and Q^* to assume values relative to an initial condition of unity. Also, this procedure allows the initial flow Q_0 to be expressed in terms of the dimensionless failure rate λ^* . This normalizing procedure is utilized for convenience in the presentation of results.

Initial Conditions. - Immediately prior to the initiation of the breach, the depths and velocities along the reservoir are those of a steady, gradually varied flow having a flowrate of Q_0 . The flow profile is either M1 or S1 backwater curve depending upon S_0 being either mild (See Fig. 3) or steep, for the steady flow rate Q_0 . In either case, the flow is subcritical in the portion of the reservoir with storage that contributes to the outflow when the dam is breached.

Referring to Fig. 1, depth and velocities at δx intervals of length along the reservoir may be computed from the steady, gradually varied flow equation (5, 15) which expressed in difference form, is

$$\frac{\delta(y+v^2/2g)}{\delta x} = S_0 - S_f \dots\dots\dots(21)$$

where S_f is defined as the average friction slope along the δx reach,

i.e.

$$S_f = \frac{(S_{fI} + S_{fII})}{2} \dots\dots\dots(22)$$

Substitution of the previously defined dimensionless variables and Eq. 22 into Eq. 21 and rearranging, yields the following dimensionless

equation

$$(F_g + y_{II}^*) (c_1 y_{II}^* - 2c_2 y_{II}^* + c_2 y_{II}^{*2})^{10/3} + G_1 (c_1 y_{II}^* - 2c_2 y_{II}^* + c_2 y_{II}^{*2})^{4/3} - G_2 (c_1 - 2c_2 + c_3 y_{II}^*)^{4/3} = 0 \dots \dots \dots (23)$$

in which

$$F_g = \frac{S_o L}{N\eta} - y_{II}^* - \frac{G_1}{(c_1 y_{II}^* - 2c_2 y_{II}^* + c_2 y_{II}^{*2})^2} - \frac{G_2 (c_1 - 2c_2 + c_3 y_{II}^*)^{4/3}}{(c_1 y_{II}^* - 2c_2 y_{II}^* + c_2 y_{II}^{*2})^{10/3}} \dots \dots \dots (24)$$

$$G_1 = \frac{Q_o^2}{2g\eta^3} \dots \dots \dots (25)$$

$$G_2 = \frac{\eta^2 L Q_o^2}{4.42 N \eta^{13/3}} \dots \dots \dots (26)$$

and N is the number of δx reaches along the reservoir, i.e.

$$N = \frac{L}{\delta x} \dots \dots \dots (27)$$

If y_{II}^* is known, Eq. 23, has only one unknown variable, y_I^* , which may be determined by Newton's Iteration Technique (10, 11).

The Newton Technique is an iterative method for solving a nonlinear equation of the form, $f(x') = 0$, by generating a sequence of successive approximations which, if a proper initial value of x' is used, converges to a desired root of the equation. The recurrence formula is

$$x'_{k+1} = x'_k - \frac{f(x'_k)}{f'(x'_k)} \dots \dots \dots (28)$$

in which $f'(x'_k) = \frac{df}{dx'_k}$ and the k and k+1 subscripts indicate the kth

and $(k+1)^{th}$ approximate values of the desired root (6).

The first δx reach, for which y_I^* is sought, is located immediately upstream of the downstream boundary, hence $y_{II}^* = 1$. The first approximation for y_I^* is simply taken as y_{II}^* . After y_I^* has been computed to within a prescribed error tolerance, v_I^* is computed from the following

$$v_I^* = \frac{(c_1 - c_2)}{(c_1 y_I^* - 2c_2 y_I^* + c_2 y_I^{*2})} \dots\dots\dots(29)$$

Proceeding upstream from the downstream boundary, depths and velocities are computed for sections located at δx intervals along the reservoir, by replacing the value of y_{II}^* in Eq. 23 with the recently computed y_I^* and repeating the above procedure. This process is repeated until all desired values of y^* and v^* are determined. These become the initial conditions which are necessary to start the procedure for solving the St. Venant equations.

Steady State Parameters. - The following steady state dimensionless parameters are used to monitor the type of flow regime at the upstream boundary

$$y_n^* = \frac{y_n}{\eta} \quad y_c^* = \frac{y_c}{\eta} \quad y_s^* = \frac{y_s}{\eta} \dots\dots\dots(30)$$

where y_n is the normal depth, y_c the critical depth, and y_s the sequent depth of the normal depth y_n , all for a steady flow of Q_o .

The normal depth y_n^* is obtained by applying Manning's equation to the flow at a section. Thus,

$$\frac{Q_o n}{1.49 S_o^{1/2}} (c_1 - 2c_2 + c_3 y_n^*)^{2/3} - [(c_1 y_n^* - 2c_2 y_n^* + c_2 y_n^{*2}) \eta]^{5/3} = 0 \dots\dots\dots(31)$$

which is solved for y_n^* by Newton's technique where the first approximation for y_n^* is determined by tacitly assuming the reservoir is a wide channel. Thus,

$$y_{n1}^* = \left[\frac{Q_o n}{1.49 S_o^{1/2} (c_1 - c_2)} \right]^{3/5} / \eta \dots \dots \dots (32)$$

Upon applying the principle of minimum energy (5) to a flow cross section, the following equation is developed

$$\frac{Q_o}{g^{1/2}} (c_1 - 2c_2 + 2c_2 y_c^*)^{1/2} - [(c_1 y_c^* - 2c_2 y_c^* + c_2 y_c^{*2}) \eta]^{3/2} = 0$$

\dots \dots \dots (33)

where Eq. 33 is solved for y_c^* by Newton's technique with the first approximation for y_c^* taken as

$$y_{c1}^* = \left[\frac{Q_o}{g^{1/2} (c_1 - c_2)} \right]^{2/3} / \eta \dots \dots \dots (34)$$

S_o is mild and the initial backwater curve is the M1 type if

$$y_n^* > y_c^* \dots \dots \dots (35)$$

S_o is steep and the backwater curve is the S1 type if

$$y_n^* < y_c^* \dots \dots \dots (36)$$

When the latter condition prevails, the upstream boundary is repositioned downstream such that the depth y_u^* exceeds the sequent depth, y_s^* . In this way, the flow in the portion of the reservoir, for which the St. Venant equations and boundary conditions are applied, is subcritical. This procedure introduces negligible error into the simulation model,

since the sequent depth is quite small for all reservoir sizes and flowrates of practical interest. If it should be desired to simulate both the supercritical and subcritical flow upstream and downstream of the moving flow discontinuity (hydraulic jump) at the upper end of the reservoir, an explicit numerical technique known as the Lax method (11, 29, 30) can be used to solve the St. Venant equations when they are expressed in their "conservation form".

The sequent depth y_s^* is determined by applying the momentum principle (5) to the discrete section of the reservoir at which a discontinuity occurs. Thus,

$$\frac{Q_o^2}{g\eta(c_1 y_s^* - 2c_2 y_s^* + c_2 y_s^{*2})} + \eta^2 y_s^{*2} \left(\frac{c_1}{2} - c_2 + \frac{c_2 y_s^*}{3} \right) - K_s = 0 \dots\dots\dots(37)$$

where

$$K_s = \frac{Q_o^2}{g\eta(c_1 y_n^* - 2c_2 y_n^* + c_2 y_n^{*2})} + \eta^2 y_n^{*2} \left(\frac{c_1}{2} - c_2 + \frac{c_2 y_n^*}{3} \right) \dots\dots\dots(38)$$

Eq. 37 is solved for y_s^* by Newton's technique with

$$y_{s1}^* = \frac{y_n^*}{2} \left(\sqrt{1 + \frac{8Q_o^2 v_n^{*2}}{g\eta^3 (c_1 - c_2)^2 y_n^*}} - 1 \right) \dots\dots\dots(39)$$

where

$$v_n^* = \frac{(c_1 - c_2)}{(c_1 y_n^* - 2c_2 y_n^* + c_2 y_n^{*2})} \dots\dots\dots(40)$$

Numerical Solution of St. Venant Equations. - The St. Venant equations defy a closed-form solution; however, they may be solved by

numerical techniques such as the explicit method (3,7,11,13,14,16,18, 21,22,26,27), the implicit method (1,3,7,18) and the method of characteristics with a characteristic network (2,3,7,9,11,17,19,28,31) and a rectangular network (4,8,19,23,28,33). Each of the techniques offer particular advantages and disadvantages (11,18). The method of characteristics with a characteristic network is used herein because of its inherent numerical stability and the ease with which boundary conditions may be introduced into the solution procedure. Also, the prismatic geometry of the idealized reservoir and the desirability of obtaining solutions at only the upstream and downstream boundaries lend to the selection of the method of characteristics.

Characteristic Equations. - In the method of characteristics, the two St. Venant partial differential equations are converted into four ordinary differential equations, called "characteristic equations", which may be numerically integrated subject to specified boundary conditions. The conversion is accomplished by forming a linear combination of Eqs. 13 and 14 through the use of a multiplier, ψ (4,11, 19,24,27,28). Thus,

$$\frac{\partial y^*}{\partial t^*} + K_1 D^* \frac{\partial v^*}{\partial x^*} + v^* \frac{\partial y^*}{\partial x^*} + \psi \left(\frac{\partial v^*}{\partial t^*} + v^* \frac{\partial v^*}{\partial x^*} + K_2 \frac{\partial y^*}{\partial x^*} + \frac{K_3 |v^*| v^*}{R^{*4/3}} - K_4 \right) = 0 \dots\dots\dots (41)$$

Upon rearranging Eq. 41 such that partial derivatives of y^* and v^* are grouped separately, i.e.

$$\psi \left[\frac{\partial v^*}{\partial t^*} + (v^* + \frac{K_1 D^*}{\psi}) \frac{\partial v^*}{\partial x^*} \right] + \left[\frac{\partial y^*}{\partial t^*} + (v^* + \psi K_2) \frac{\partial y^*}{\partial x^*} \right] + \psi \left(\frac{K_3 |v^*| v^*}{R^{*4/3}} - K_4 \right) = 0 \dots\dots\dots(42)$$

The bracketed quantities may be made total derivatives, i.e. $\frac{dv^*}{dt^*}$ and $\frac{dy^*}{dt^*}$

if $v^* + \frac{K_1 D^*}{\psi} = \frac{dx^*}{dt^*} \dots\dots\dots(43)$

and $v^* + K_2 \psi = \frac{dx^*}{dt^*} \dots\dots\dots(44)$

The simultaneous solution of Eqs. 43 and 44 yields ψ . Thus,

$$\psi = \pm \sqrt{\frac{K_1 D^*}{K_2}} \dots\dots\dots(45)$$

Substitution of Eq. 45 into Eqs. 42-44 and rearranging, yields

$$\frac{dv^*}{dt^*} - \sqrt{\frac{K_2}{K_1 D^*}} \frac{dy^*}{dt^*} + \frac{K_3 |v^*| v^*}{R^{*4/3}} - K_4 = 0 \dots\dots\dots(46)$$

$$\frac{dx^*}{dt^*} = v^* - \sqrt{K_1 K_2 D^*} \dots\dots\dots(47)$$

} C-

$$\frac{dv^*}{dt^*} + \sqrt{\frac{K_2}{K_1 D^*}} \frac{dy^*}{dt^*} + \frac{K_3 |v^*| v^*}{R^{*4/3}} - K_4 = 0 \dots\dots\dots(48)$$

$$\frac{dx^*}{dt^*} = v^* + \sqrt{K_1 K_2 D^*} \dots\dots\dots(49)$$

} C+

Eqs. 46 and 47 are associated with the C- characteristic curves in the x^*-t^* solution plane, shown in Fig. 4; Eqs. 48 and 49 are associated with the C+ characteristic curves. It is noted that Eqs. 46 and 48 contain no partial derivatives; however, the additional Eqs. 47 and 49 are required since Eqs. 46 and 48 are valid only along the curves defined by the dx^*/dt^* expressions. All four equations are valid at intersection points, such as p, in the x^*-t^* plane. Thus, if the values of x^*, t^*, y^* and v^* are known at points, l and r, a numerical integration of the equations will produce the values of x^*, t^*, y^* , and v^* at point p. In this way, the values associated with all intersection points in the x^*-t^* plane are determined sequentially from left to right while progressing upward in the t^* -direction.

The numerical integration of Eqs. 46-49 may be accomplished by various finite-difference approximations with different orders of accuracy (2,3,11,19,29). It was found that a simple first-order approximation of the form

$$\int_{x_r^*}^{x_p^*} f(x^*) dx^* \approx f(x_r^*) (x_p^* - x_r^*) \dots \dots \dots (50)$$

provided sufficient accuracy since the variation of v^* and y^* with x^* and t^* is relatively small for a flow produced by a gradual breach.

Upon applying Eq. 50 to Eqs. 46-49 and rearranging, four equations, which are linear with respect to the variables at location p, are obtained as follows

FIGURE 4. $x^* - t^*$ PLANE WITH CHARACTERISTIC NETWORK

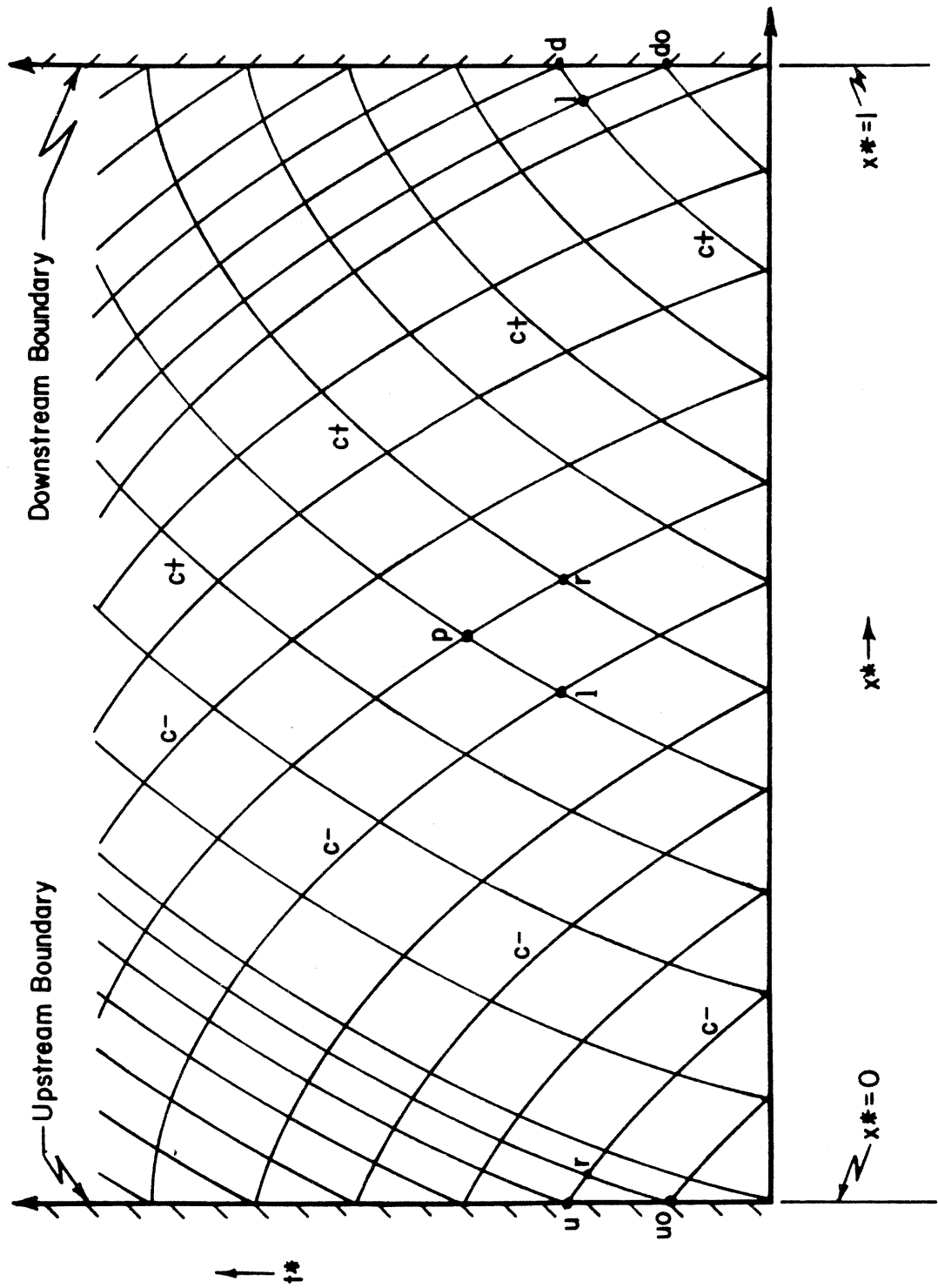


FIGURE 4.

$$v_p^* - v_r^* - F_2(y_p^* - y_r^*) + F_3(t_p^* - t_r^*) = 0 \dots\dots\dots (51)$$

$$x_p^* - x_r^* = F_1(t_p^* - t_r^*) \dots\dots\dots (52)$$

} C-

$$v_p^* - v_1^* + F_5(y_p^* - y_1^*) + F_6(t_p^* - t_1^*) = 0 \dots\dots\dots (53)$$

$$x_p^* - x_1^* = F_4(t_p^* - t_1^*) \dots\dots\dots (54)$$

} C+

where $F_1 = v_r^* - \sqrt{K_1 K_2 D_r^*} \dots\dots\dots (55)$

$$F_2 = \sqrt{\frac{K_2}{K_1 D_r^*}} \dots\dots\dots (56)$$

$$F_3 = \frac{K_3 v_r^* |v_r^*|}{R_r^{* 4/3}} - K_4 \dots\dots\dots (57)$$

$$F_4 = v_1^* + \sqrt{K_1 K_2 D_1^*} \dots\dots\dots (58)$$

$$F_5 = \sqrt{\frac{K_2}{K_1 D_1^*}} \dots\dots\dots (59)$$

$$F_6 = \frac{K_3 v_1^* |v_1^*|}{R_1^{* 4/3}} - k_4 \dots\dots\dots (60)$$

Substitution of y_1^* and y_r^* for y^* in Eq. 10 and 11, provides the values of D_1^* , D_r^* , R_1^* , R_r^* .

Upstream Boundary. - The V-breach is assumed to occur during a short duration of time relative to the time base of the reservoir inflow hydrograph. The inflow occurs only at the upper reach of the idealized reservoir such that the reservoir is not subjected to any lateral inflow. Hence, the inflow to the reservoir may be considered

relatively constant throughout the formation of the breach, and the upstream boundary condition is expressed as a constant inflow, i.e.

$$Q_u = Q_u(t) = Q_o \dots\dots\dots(61)$$

and in dimensionless form,

$$Q_u^* = \frac{Q_u}{Q_o} = 1 \dots\dots\dots(62)$$

Thus, from continuity considerations

$$v_u^* = \frac{Q_u^*(c_1 - c_2)}{(c_1 y_u^* - 2c_2 y_u^* + c_2 y_u^{*2})} \dots\dots\dots(63)$$

The value of x_u^* is known since it represents the location of the upstream boundary; hence, t_u^* may be computed from the C- Eq. 52,

$$t_u^* = t_r^* + \frac{(x_u^* - x_r^*)}{F_1} \dots\dots\dots(64)$$

Substitution of Eq. 63 into the C- Eq. 51 yields

$$(F_u - F_2 y_u^*)(c_1 y_u^* - 2c_2 y_u^* + c_2 y_u^{*2}) + Q_u^*(c_1 - c_2) = 0 \dots\dots\dots(65)$$

where $F_u = -v_r^* + F_2 y_r^* + F_3 (t_u^* - t_r^*) \dots\dots\dots(66)$

Eq. 65 may be solved for y_u^* by Newton's technique with

$$y_{u1}^* = y_{u0}^* \dots\dots\dots(67)$$

where the u_0 subscript is associated with the previously computed upstream boundary point shown in Fig. 4. The value for v_u^* is computed from Eq. 63.

Interior Points. - The unknown values of x^* , t^* , y^* and v^* at any interior point designated by a p subscript may be easily obtained from the simultaneous solution of the four linear Eqs. 51-54.

Thus,

$$t_p^* = \frac{(x_1^* - x_r^* + F_1 t_r^* - F_4 t_1^*)}{(F_1 - F_4)} \dots\dots\dots(68)$$

$$x_p^* = x_1^* + F_4 (t_p^* - t_1^*) \dots\dots\dots(69)$$

$$y_p^* = \frac{[v_1^* - v_r^* + F_2 y_r^* + F_5 y_1^* + F_3 (t_p^* - t_r^*) - F_6 (t_p^* - t_1^*)]}{(F_2 + F_5)} \dots\dots\dots(70)$$

$$v_p^* = v_1^* - F_5 (y_p^* - y_1^*) - F_6 (t_p^* - t_1^*) \dots\dots\dots(71)$$

Downstream Boundary. - The location of the downstream boundary is known; hence,

$$x_d^* = l \dots\dots\dots(72)$$

and t_d^* may be computed from the C+ Eq. 54, i.e.

$$t_d^* = t_1^* + \frac{(x_d^* - x_1^*)}{F_4} \dots\dots\dots(73)$$

The downstream boundary condition is given by stage-discharge relationships for the spillway and the V-breach. The elevation of the spillway crest η_{sp}^* is constant, however, the elevation of the bottom of the V-breach η_v^* is a function of t_d^* , η_{1t}^* , η_{1b}^* , and λ^* . The following step-functions express this variation of η_v^* .

$$\text{If } \eta_{vo}^* \geq \eta_{1t}^* \dots\dots\dots(74)$$

$$\text{then } \eta_v^* = \eta_{vo}^* - \lambda^* (t_d^* - t_{do}^*) \dots\dots\dots(75)$$

however if $\eta_v^* < \eta_{1t}^*$ (76)

then $\eta_v^* = \eta_{1t}^* - \frac{[\lambda^* t_d^* - (\eta_{vo}^* - \eta_{1t}^*)]}{K_\lambda}$ (77)

If $\eta_{1b}^* \leq \eta_{vo}^* < \eta_{1t}^*$ (78)

then $\eta_v^* = \eta_{vo}^* - \frac{\lambda^*}{K_\lambda} (t_d^* - t_{do}^*)$ (79)

however if $\eta_v^* < \eta_{1b}^*$ (80)

then $\eta_v^* = \eta_{1b}^* - [\lambda^* t_d^* - K_\lambda (\eta_{vo}^* - \eta_{1b}^*)]$ (81)

If $0 \leq \eta_{vo}^* < \eta_{1b}^*$ (82)

then $\eta_v^* = \eta_{vo}^* - \lambda^* (t_d^* - t_{do}^*)$ (83)

however if $\eta_v^* < 0$ (84)

then $\eta_v^* = 0$ (85)

The second subscript, o, indicates that the subscripted variable is the previously computed boundary point as shown in Fig. 4.

The velocity at the downstream boundary is expressed in terms of the discharges of the spillway and the V-breach, and the reservoir cross-section, i.e.

$$v_d^* = \frac{[K_5 (y_d^* - \eta_v^*)^{5/2} + K' K_6 (y_d^* - \eta_{sp}^*)^{3/2}] (c_1 - c_2)}{(c_1 y_d^* - 2c_2 y_d^* + c_2 y_d^{*2})} \dots (86)$$

where $K' = 1$ (87)

if $y_d^* > \eta_{sp}^*$ (88)

and $K' = 0$ (89)

if $y_d^* < \eta_{sp}^*$ (90)

and $K_5 = C_v \eta^{5/2} / Q_o$ (91)

$K_6 = C_{sp} \eta^{3/2} / Q_o$ (92)

$C_v = 4.28 c_v \tan \frac{\phi}{2}$ (93)

$C_{sp} = 5.36 c_{sp} L_{sp} = Q_o / [n(1-\eta_{sp}^*)]^{3/2}$ (94)

Substitution of Eq. 86 into the C+ Eq. 53 yields

$$K_5 (y_d^* - \eta_v^*)^{5/2} + K' K_6 (y_d^* - \eta_{sp}^*)^{3/2} + \frac{(c_1 y_d^{*2} - 2c_2 y_d^* + c_2 y_d^{*2})(F_4 y_d^* + F_d)}{(c_1 - c_2)}$$

= 0(95)

where $F_d = -v_1^* - F_5 y_1 + F_6 (t_d^* - t_1^*)$ (96)

Eq. 95 may be solved for y_d^* by Newton's technique with

$y_{d1}^* = y_{do}^*$ (97)

Then, v_d^* is computed from Eq. 86 and the reservoir release discharge

Q_d^* is computed from the following

$$Q_{d1}^* = \frac{v_d^* (c_1 y_d^{*2} - 2c_2 y_d^* + c_2 y_d^{*2})}{(c_1 - c_2)}$$

.....(98)

Optimization of Retarding Layer Location. - When a dam does not have an erosion retarding layer, the maximum possible reservoir release Q_{dmp}^* due to a breached dam occurs at η_{vmp}^* which may be at any elevation within the dam; this elevation depends upon the magnitude of the reservoir surface area, bottom slope, the failure rate λ and C_v . When Q_{dmp}^* occurs, the two factors controlling the rate of discharge through the breach, namely the head $(y_d^* - \eta_v^*)$ on the breach and the flow area of the breach must assume their maximum simultaneous values. Thereafter and until practically all of the storage above y_n^* is released, the reservoir surface level y_d decreases since the reservoir outflow Q_d^* exceeds the reservoir inflow Q_u .

The optimum elevation η_{ltOp}^* of the retarding layer is defined herein as that elevation which minimizes the maximum reservoir outflow Q_{dm}^* . Thus, by optimally positioning the retarding layer, a maximum reduction in Q_{dmp}^* is achieved. Such a reduction, denoted as QR, is defined as a percentage reduction, i.e.

$$QR = \frac{(Q_{dmp}^* - Q_{dm}^*) 100}{Q_{dmp}^*} \dots \dots \dots (99)$$

An iterative procedure is utilized to determine η_{ltOp}^* within an acceptable accuracy. Initially, the breach is simulated with η_{lt}^* equal to zero, i.e. the dam does not have a retarding layer; and Q_{dmp}^* is determined. Then, the breach is simulated with the retarding layer positioned at $\eta_{lt_{k+1}}^*$ which is defined as

$$\eta_{lt_{k+1}}^* = \eta_{lt_k}^* + \delta \eta_{lt}^* \dots \dots \dots (100)$$

where the k subscript denotes the number of iterations using an incremental increase of $\delta\eta_{lt}^*$, and $\eta_{lt_1}^* = \eta_{vmp}^*$. The simulation of the breach, with the retarding layer positioned at $\eta_{lt_{k+1}}^*$, is continued until $\eta_v^* < \eta_{vmp}^*$ since all subsequent Q_d^* must be less than that occurring when η_v^* has reached η_{vmp}^* . When the dam has a retarding layer that is positioned above the η_v^* at which Q_{dmp}^* occurred, Q_{dm}^* will be less than Q_{dmp}^* since the retarding layer allows the water level in the reservoir to recede while the area of the breach remains relatively constant. Thus, Q_{dm}^* will occur at some η_v^* which is greater than η_{vmp}^* .

The reduction in Q_{dmp}^* , denoted as QR, is a function of the position η_{lt}^* of the retarding layer. A typical relationship between QR and η_{lt}^* is shown in Fig. 5. The function, $QR = QR(\eta_{lt}^*)$, was investigated for a variety of reservoir parameters (L , η , Q_o , λ , etc.) and was found to contain only one maximum value. Thus, the difficulties encountered when a function contains more than one maximum (peak) is avoided in the iterative search for η_{ltOp}^* .

Using an incremental increase $\delta\eta_{lt}^*$, QR_k is computed for each η_{lt_k} position of the retarding layer until QR_{k+1} is greater than QR_k . When this occurs, as noted in Fig. 5, QR_{max} and the corresponding η_{ltOp}^* exists for a value of η_{lt}^* less than $\eta_{lt_{k+1}}^*$. Then QR_{k+2} and QR_{k+3} are computed, and the final location of QR_{max} is easily obtained graphically by extending smooth curves through all the computed points $(QR, \eta_{lt_k}^*)$.

Modifications to Model. - Modifications may readily be made to the above numerical simulation model to accommodate reservoir geometries,

FIGURE 5. TYPICAL VARIATION OF THE PERCENT REDUCTION (QR) IN
THE MAXIMUM POSSIBLE RESERVOIR RELEASE WITH THE
LOCATION (η_{1t}^*) OF THE EROSION RETARDING LAYER

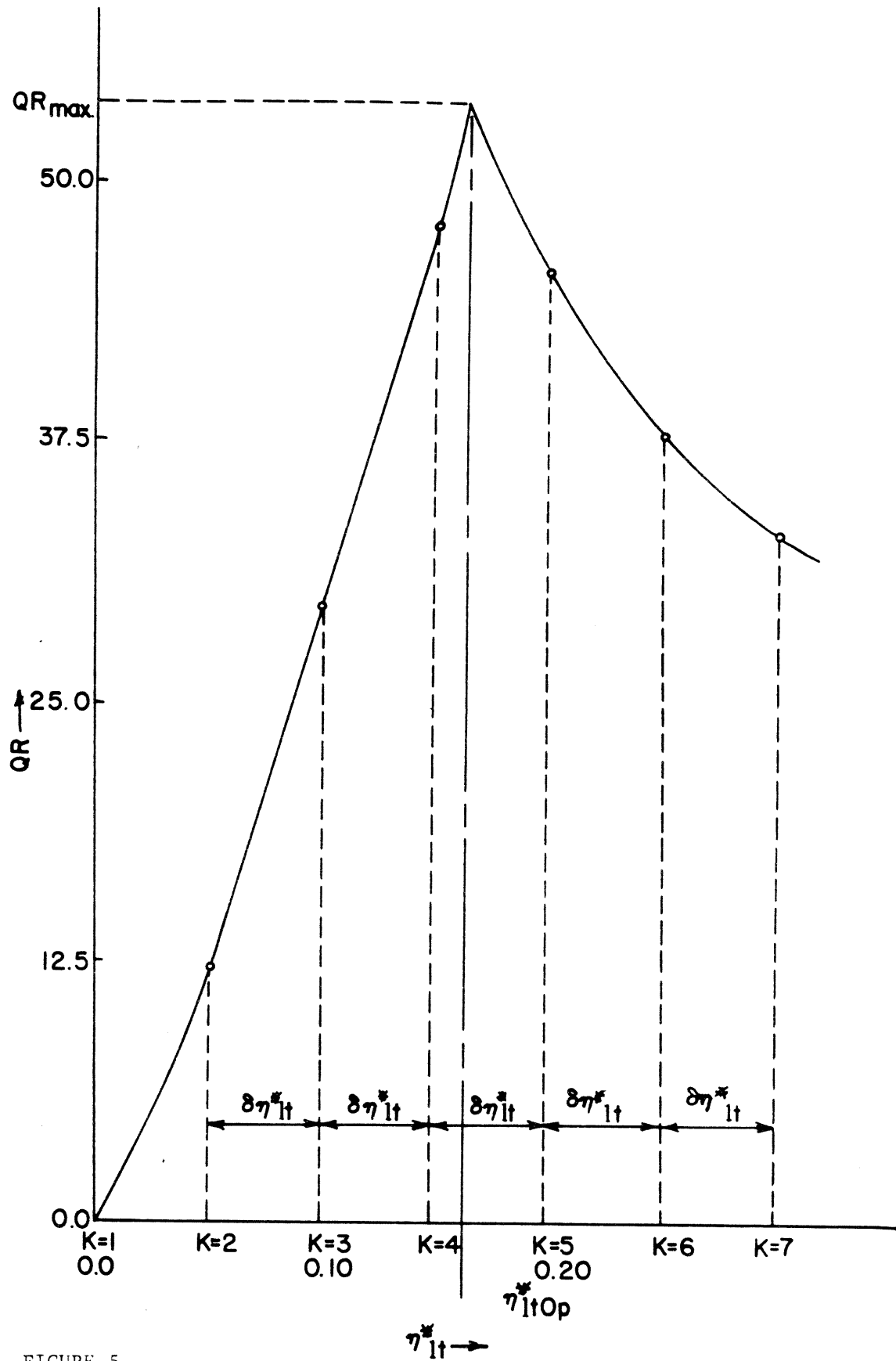


FIGURE 5.

bottom slopes, breach geometries, upstream and downstream boundary conditions, and breach dynamics which differ from those treated herein.

Rectangular or triangular reservoir cross sections may be simulated by letting $z=0$ or $z=L/(2\pi\eta)$, respectively. Other cross-sectional geometries may be handled by properly defining A , D , and R . The reservoir bottom slope S_o may be defined other than by Eq. 4 and thus be independent of η and L . Breach geometries, other than a V-shape may be simulated by defining the cross-sectional area of the breach as a function of η_v^* .

A principal spillway and/or a different type of emergency spillway may be incorporated into the downstream boundary condition by defining their respective stage-discharge relationships and elevations. The discharge coefficients C_{sp} and C_v of the spillway and V-breach may be expressed as functions of y_d , η_{sp} , and or η_v rather than assumed to be constants.

The upstream boundary condition may be changed to a stage or discharge hydrograph by specifying the relationship between the upstream stage or discharge with time.

The initiation of the breach may be defined so as to occur when the depth y_d^* at the downstream boundary exceeds η^* by a specified amount. The failure rate λ may be described by various mathematical functions other than Eqs. 5 and 6.

EXPERIMENTAL SIMULATION MODEL

An experimental simulation model was developed to check the accuracy of the numerical model. A vertical dam, consisting of two adjacent,

metal plates, was installed near the midpoint of a 40 ft. long by 2 ft. wide Plexiglas flume. The thin metal plates were shaped such that a V-opening was formed at the centerline of the dam when the plates were moved in opposite horizontal directions parallel to the flume cross section. The ϕ angle of the V-opening (breach) remained constant throughout its formation and gradual enlargement. A magnetic clutch provided an instantaneous application of a variable speed drive-unit to a cable-pulley system which pulled the metal plates apart. This system permitted the V-breach to be formed at any desired rate λ from 0.0 - 0.15 fps.

The simulated reservoir formed by the two-dimensional metal dam was of rectangular cross section having a depth y_d of 1.704 ft. at the dam. A steady inflow Q_o was introduced at the upstream end of the reservoir and the same quantity was released from the reservoir through a small V-opening at the top of the dam. This outflow simulated the steady spillway discharge assumed to occur prior to an over-topping failure. The V-opening was enlarged at a known rate λ ; this simulated the formation of a gradual V-shaped breach. A timed-pause in the formation of the V-breach simulated the effect of an erosion retarding layer.

The discharge coefficient C_v of the V-breach was determined for numerous steady flows at various settings of the metal plates so as to provide steady state discharge coefficients which spanned the entire range of possible V-openings (η_v) and heads ($y_d - \eta_v$) on the V-breach. The discharge coefficient was found to vary with both η_v and y_d . This variation was expressed in the form

$$C_v = K_{c1} \left(\frac{y_d - \eta_v}{\eta_v} \right)^{-K_{c2}} \dots \dots \dots (101)$$

where K_{c1} varied from 1.580 to 1.634 and K_{c2} varied from 0.001 to 0.098; both are functions of $(y_d - \eta_v)$ and η_v .

Timers and staff gauges, positioned at stations 1.00 and 10.00 ft. upstream from the dam, were continuously monitored via movie cameras. This provided stage hydrographs at the selected stations. Total outflow Q_t from the reservoir was determined for a specified duration of time t_f after the time t_o at which movement of the metal plates was initiated. Thus,

$$Q_t = Q_o t_f + TL(y_{d_{t_o}} - y_{d_{t_f}}) \dots \dots \dots (102)$$

NUMERICAL RESULTS

Comparison With Experimental Results. - The numerical simulation model provides results which are in satisfactory agreement with the experimental model. A typical stage hydrograph for station 1.00 is shown in Fig. 6 along with the stage as computed by the numerical model. The percent standard deviation σ_{y_d} between the experimental and numerical y_d is 1.17%, and for all experimental runs, σ_{y_d} is 0.83%. The computed outlet discharge hydrograph associated with the stage hydrograph is also shown in Fig. 6. Total outflow, as computed by the numerical model, is determined by numerically integrating the discharge hydrograph. The percent standard deviation σ_{Q_t} between the experimental and numerical total outflows is 5.1% for all experimental runs. Additional experimental-numerical stage and discharge hydrographs for this study are presented in reference (12).

FIGURE 6. STAGE AND DISCHARGE HYDROGRAPHS OF EXPERIMENTAL
RUN NO. 5

$$\lambda = 0.04975 \text{ fps} \quad t < 5.70$$

$$\lambda = 0.05620 \text{ fps} \quad t > 5.70$$

$$\eta_v(\text{Minimum}) = 0.340 \text{ ft.}$$

$$S_0 = 0.0001$$

$$n = 0.009$$

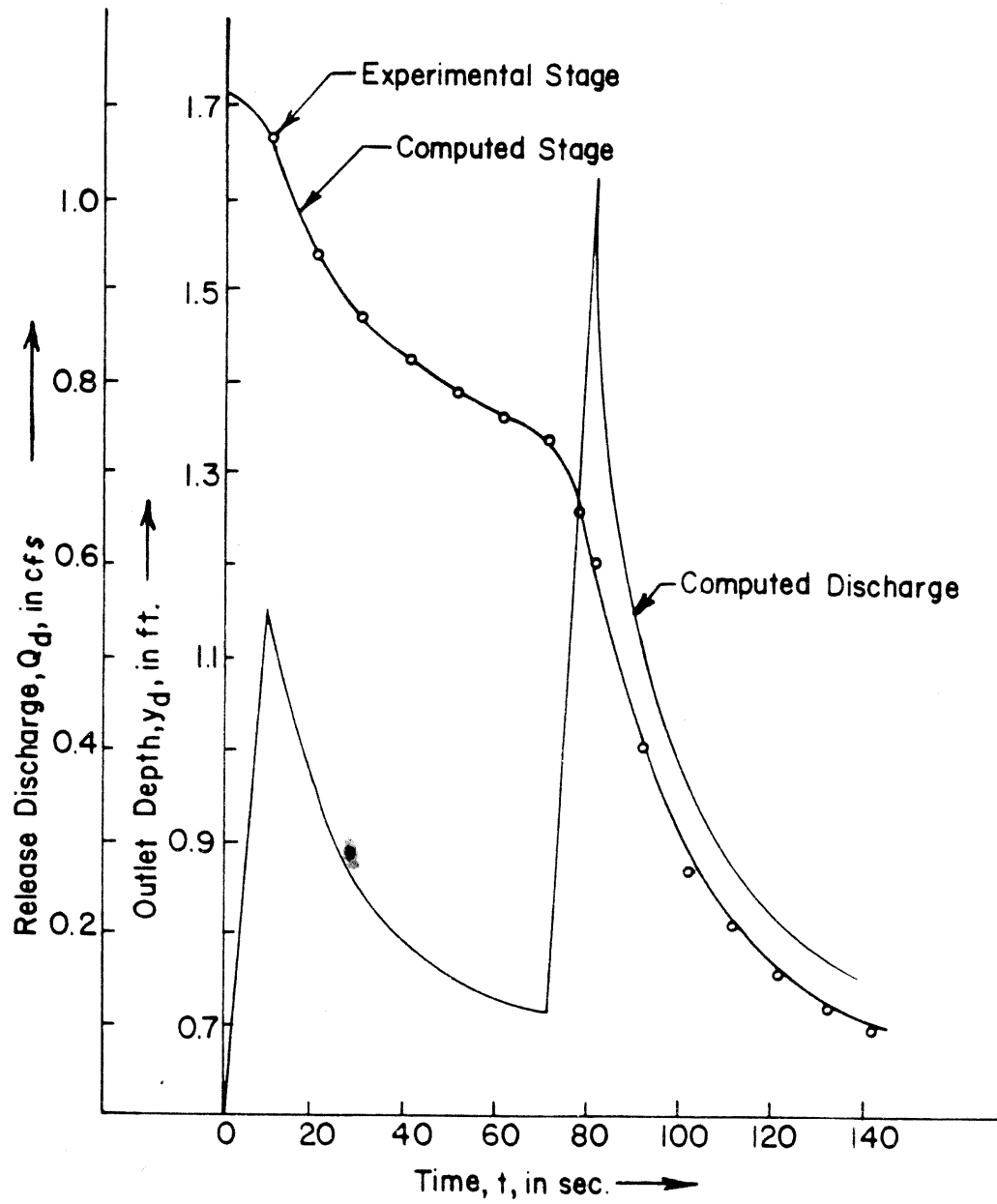


FIGURE 6.

Retarding Layer: Optimal Location and Reduction in Outflow. - Upon applying the numerical simulation model to a range of reservoir sizes, dam heights, initial flowrates, and dam failure rates, prediction curves are obtained for the dimensionless optimal elevation η_{ltOp}^* of the erosion retarding layer and the extent of its reduction QR_{max} in the reservoir outflow. The results are functions of the parameters used herein to describe the transient hydraulics associated with the gradual V-breach of an earthfill dam. These parameters consist of the following: geometric parameters ($L, K_1, \tau, \eta, \eta_{sp}$, and η_{ld}); hydraulic parameters (Q_o, n, C_v); and dynamic parameters (λ and K_λ).

The values of η_{ltOp}^* and QR_{max} are expressed as functions of the dimensionless failure rate λ^* , as defined by Eq. 19, and for specific values of L, τ, λ_c, η , and K_λ . The prediction curves for η_{ltOp}^* and QR_{max} are applicable for the "fixed parameters", $K_1=1.2, z=2, \eta_{sp}^*=0.95, \eta_{ld}^*=0.02, n=0.03$ and $C_v=2.2$. The sensitivity of the prediction curves to variations in these fixed parameters is examined in a following section.

Prediction curves for η_{ltOp}^* and QR_{max} are shown in Figures 7-12 for specific values of L, τ, K_λ and λ_c . The following example illustrates the use of the prediction curves:

When $Q_o=2,000$ cfs, $L=10,000$ ft, $\tau=10$, $\eta=100$ ft, $\lambda_c=0.01$ fps, $K_\lambda=100, K_1=1.20, z=2., \eta_{sp}^*=0.95, \eta_{ld}^*=0.02, n=0.03$, and $C_v=2.2$, the optimum elevation η_{ltOp}^* of an erosion retarding layer and the corresponding reduction QR_{max} in the maximum possible reservoir release may be obtained from Fig. 8. First, λ^* is computed from Eq. 19, i.e. $\lambda^* = \frac{(10000)(.01)}{2000} [\frac{10000}{10} - 2(100)] = 40$. Then a line is extended vertically from

FIGURE 7. RELATIONSHIP BETWEEN QR_{\max} AND η_{ltOp}^* FOR VARIOUS
VALUES OF λ^* AND $L=10,000$ ft., $\tau=10$, $\lambda_c=0.1$ fps

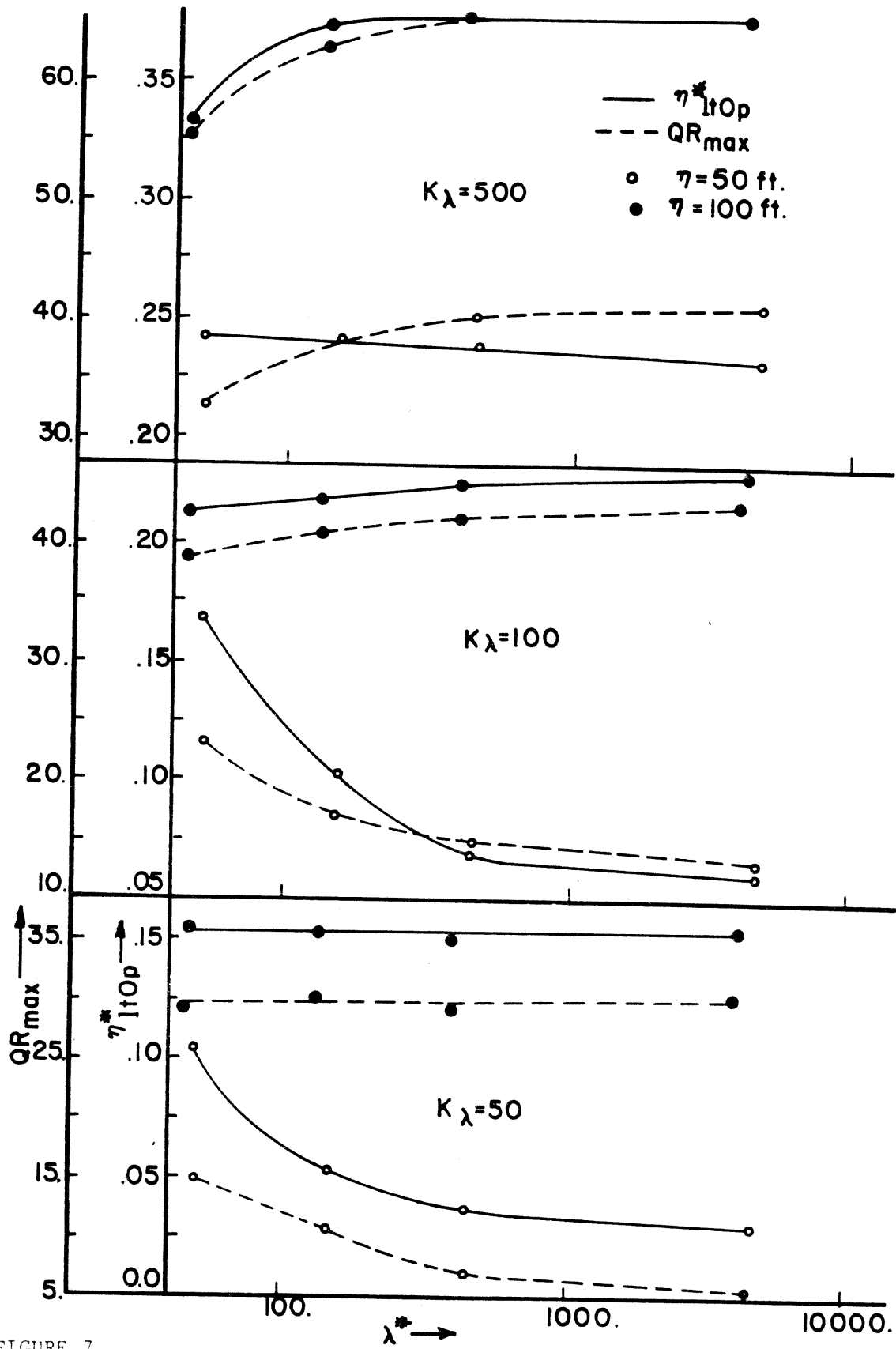


FIGURE 7.

FIGURE 8. RELATIONSHIP BETWEEN QR_{\max} AND η_{1t0p}^* FOR VARIOUS
VALUES OF λ^* AND $L=10,000$ ft., $\tau=10$, $\lambda_c=0.01$ fps

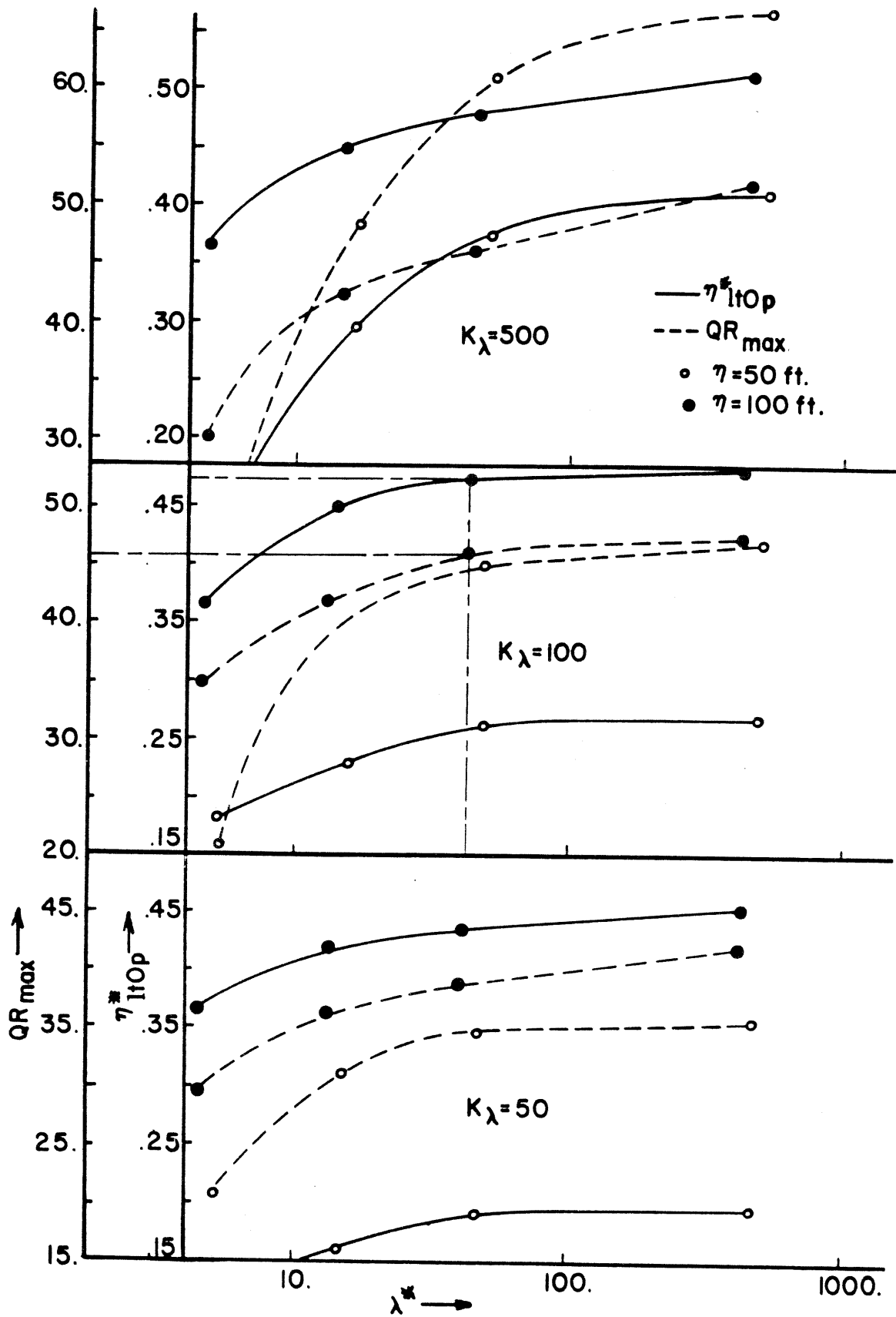


FIGURE 8.

FIGURE 9. RELATIONSHIP BETWEEN QR_{\max} AND n_{1t0p}^* FOR VARIOUS
VALUES OF λ^* AND $L=10,000$ ft., $\tau=10$, $\lambda_c=0.005$ fps

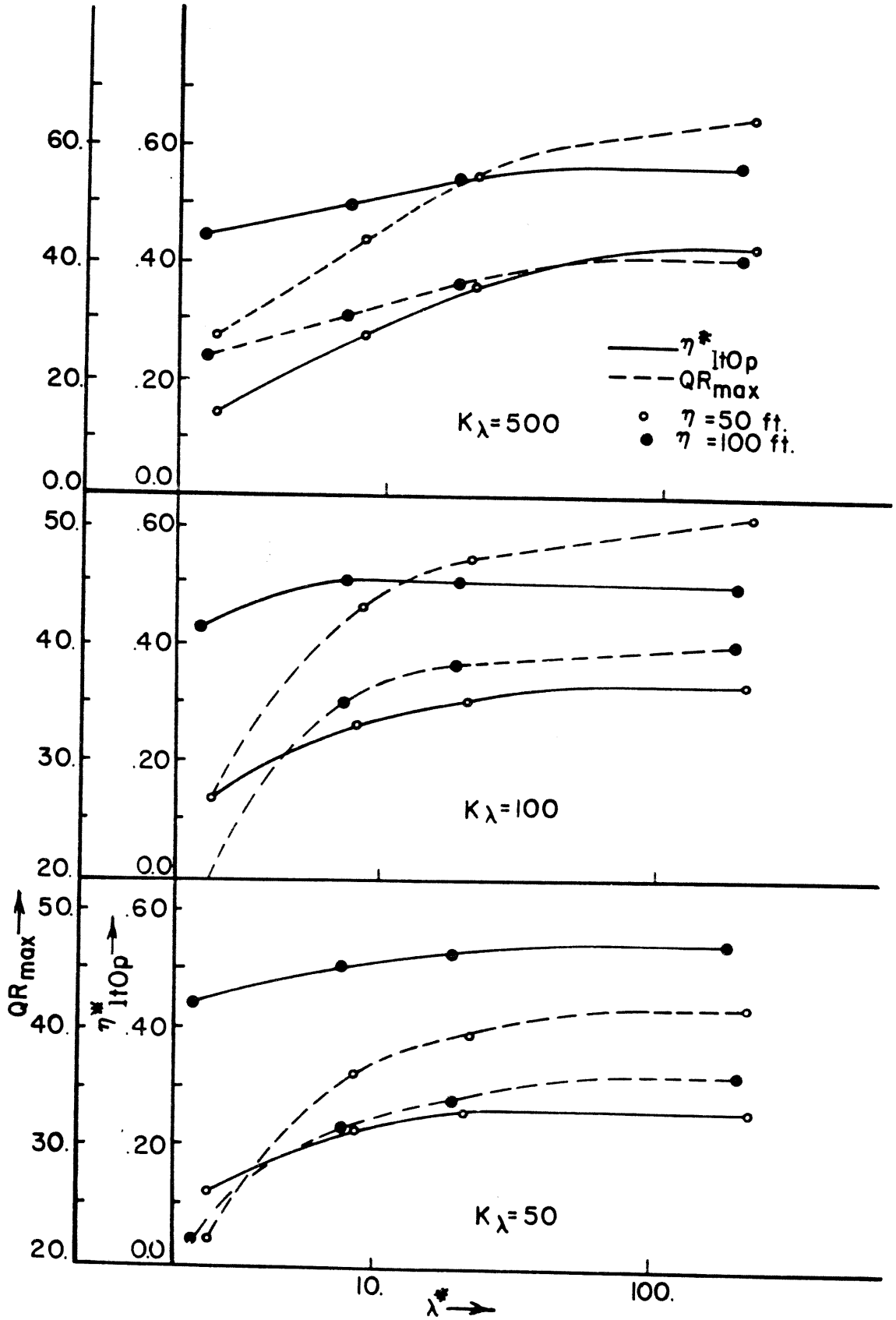


FIGURE 9.

FIGURE 10. RELATIONSHIP BETWEEN QR_{\max} AND η_{lt0p}^* FOR VARIOUS
VALUES OF λ^* AND $L=2,000$ ft., $\tau=4$, $\lambda_c=0.1$ fps

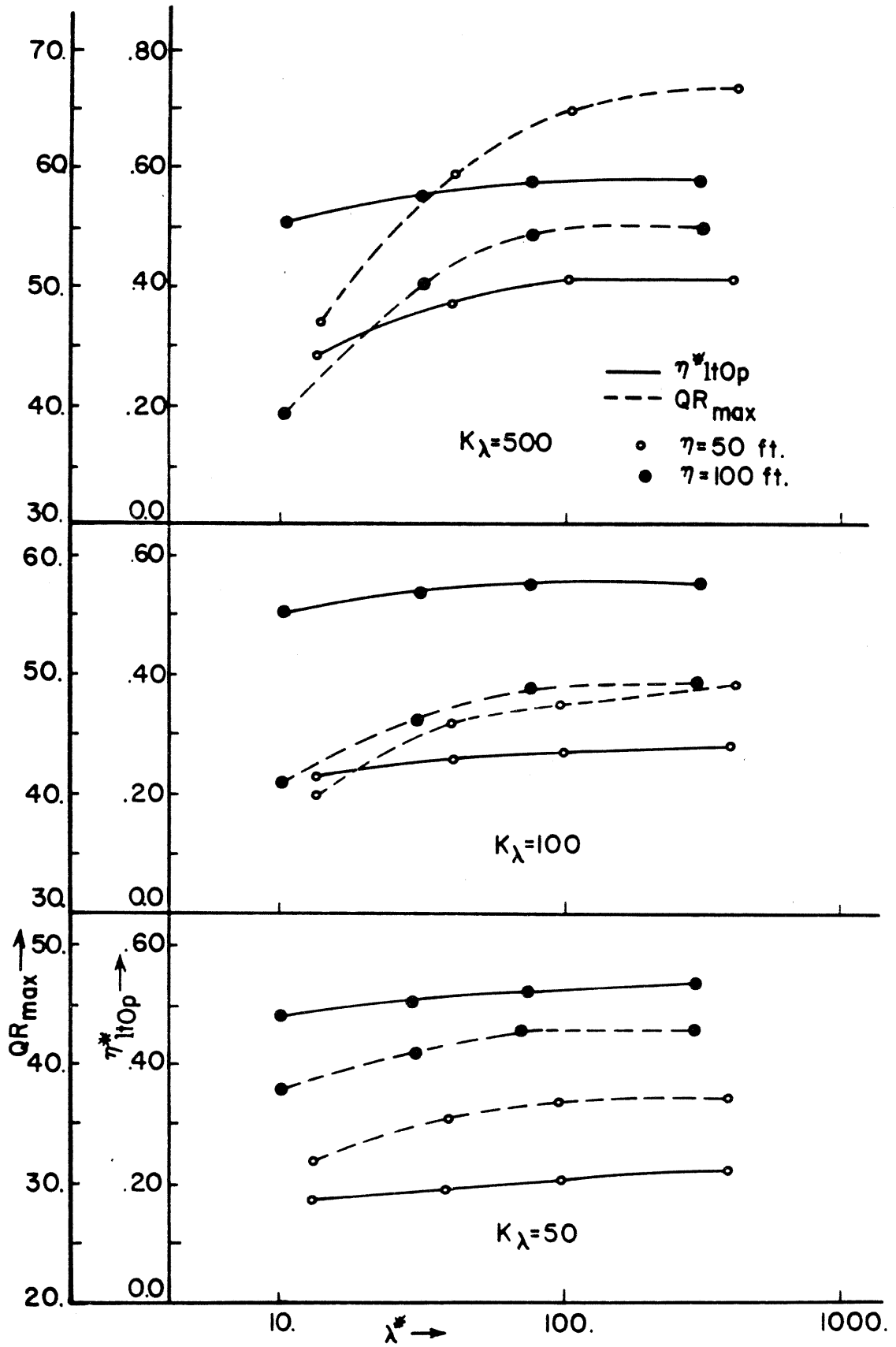


FIGURE 10.

FIGURE 11. RELATIONSHIP BETWEEN QR_{\max} AND η_{1t0p}^* FOR VARIOUS
VALUES OF λ^* AND $L=2,000$ ft., $\tau=4$, $\lambda_c=0.01$ fps

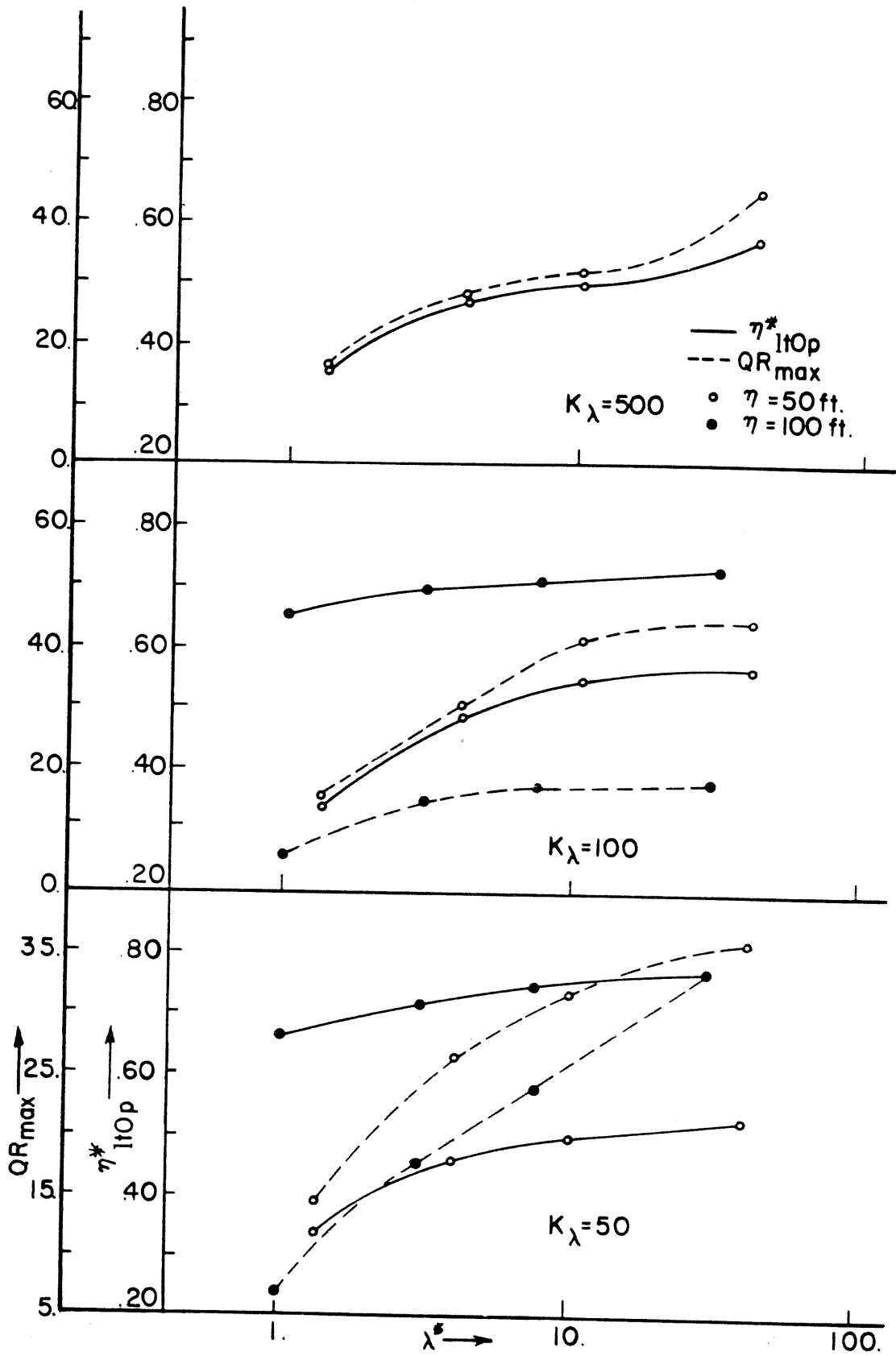


FIGURE 11.

FIGURE 12. RELATIONSHIP BETWEEN QR_{\max} AND η_{lt0p}^* FOR VARIOUS
VALUES OF λ^* AND $L=2,000$ ft., $\tau=4$, $\lambda_c=0.005$ fps

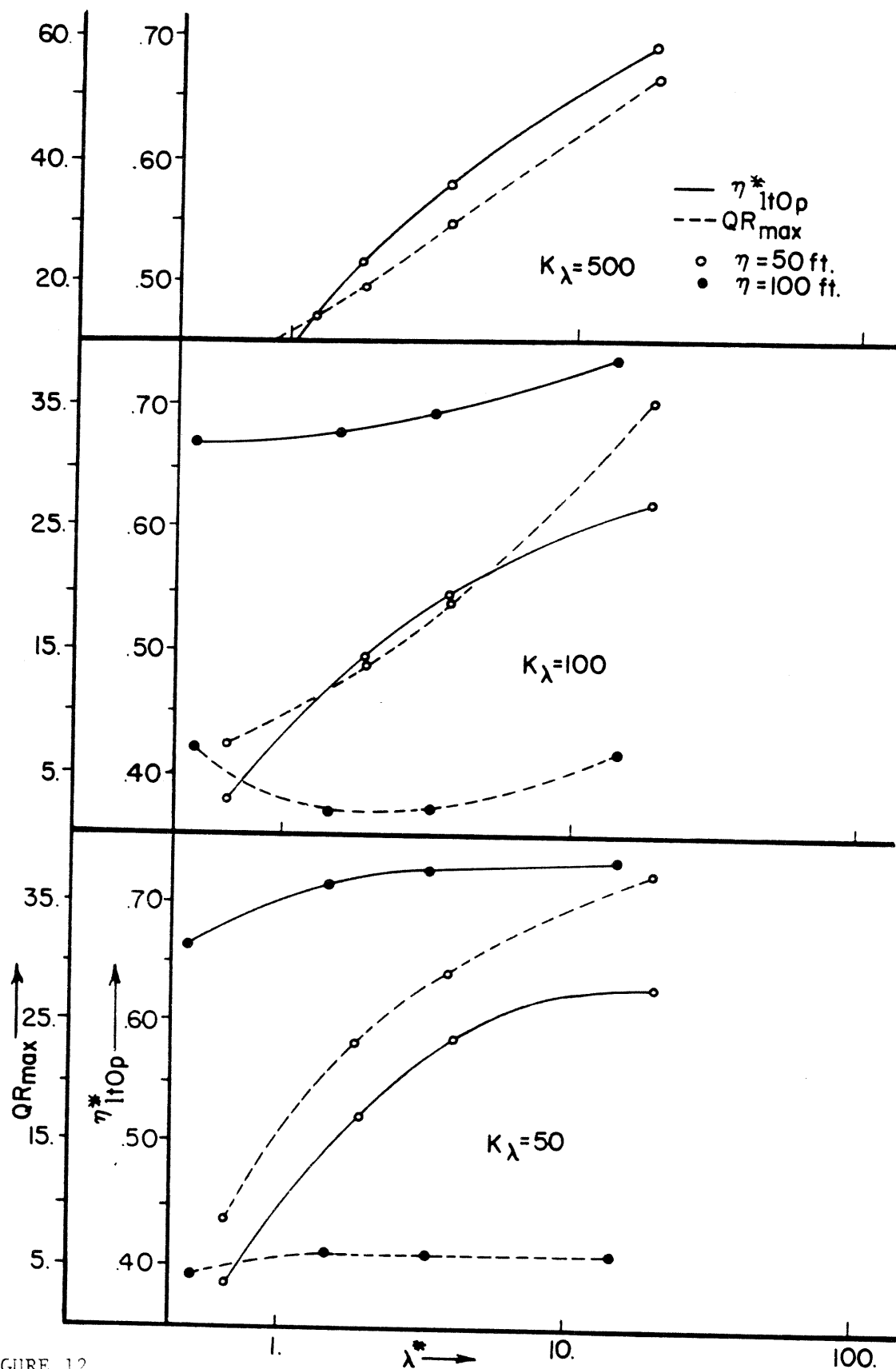


FIGURE 12.

the abscissa at $\lambda^* = 40$ to intersect the curves pertaining to $K_\lambda = 100$ and $\eta = 100$ ft. as shown in Fig. 8. Finally, the values of η_{ltOp}^* and QR_{max} are obtained by extending lines horizontally until they intersect the appropriate ordinate axis, and η_{ltOp}^* and QR_{max} are read as 0.463 and 45.8%, respectively.

Upon examining Figs. 7-12, it is evident that η_{ltOp}^* significantly varies directly with η and K_λ and inversely with L and λ_c . Also, in all except Fig. 7, η_{ltOp}^* varies directly with λ^* .

If the failure rate λ_c is very small and/or L is small, say $L = 2000$ ft., the reservoir depth as determined by the numerical model recedes at an increasing rate as the V-breach forms. Under this condition, the maximum possible reservoir release Q_{dmp}^* occurs when the rate at which the depth is receding exceeds the failure rate λ_c , i.e. Q_{dmp}^* occurs considerably before the breach achieves its maximum size. Hence, η_{ltOp}^* may assume values in the range of 0.60 to 0.75. Under this same condition of small values of λ_c and/or L , the elevation of the erosion retarding layer is critical since it is possible for the layer, if incorrectly positioned above η_{vmp}^* , to cause Q_{dm}^* to exceed Q_{dmp}^* .

In Figs. 7-12, QR_{max} assumes values in the range of 10 to 65%. This indicates that significant reductions in the maximum reservoir release from gradually breached dams may be achieved by the presence of an erosion retarding layer which is optimally located. The extent of the reduction QR_{max} is primarily related directly to the resistance of the layer to erosion, i.e. K_λ , and to λ^* .

Prediction curves for η_{ltOp}^* and QR_{max} are shown in Figs. 13 and 14 for specific values of L , τ , η , k_λ , λ_m , and y_{dm} . In these, λ is

FIGURE 13. RELATIONSHIP BETWEEN QR_{\max} AND η_{ltOp}^*
FOR VARIOUS VALUES OF λ^* AND $L=10,000$ ft., $\tau=10$,
 $\lambda_m=0.1$ fps, $y_{dm}=0.97$ ($\eta=50$ ft.), $y_{dm}=0.91$
($\eta=100$ ft.) AND λ IS AN EXPONENTIAL FUNCTION

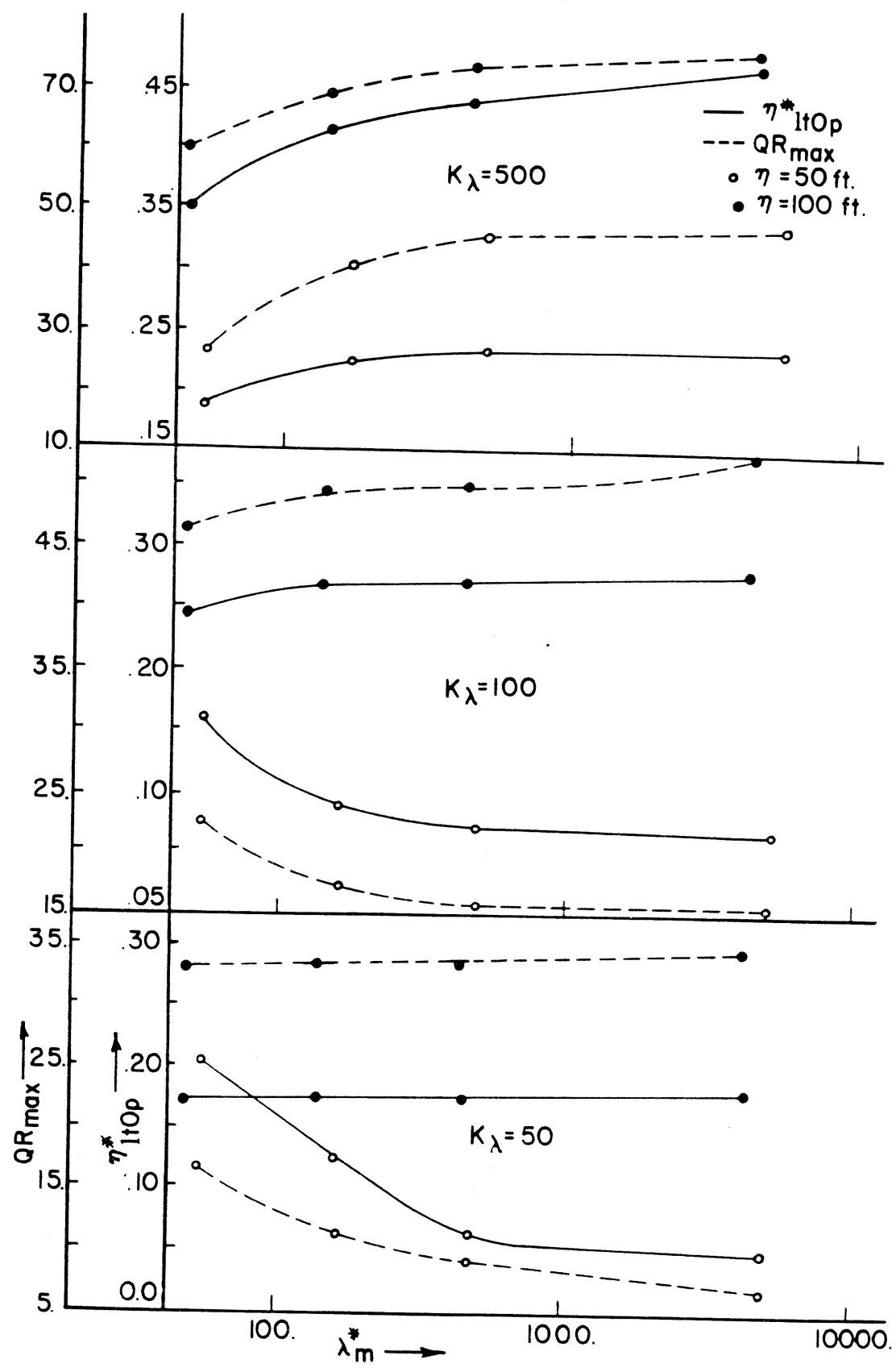


FIGURE 13.

FIGURE 14. RELATIONSHIP BETWEEN QR_{\max} AND η_{lt0p}^*
FOR VARIOUS VALUES OF λ^* AND $L=10,000$ ft., $\tau=10$,
 $\lambda_m=0.01$ fps, $y_{dm}=0.90$ ($\eta=50$ ft.), $y_{dm}=0.58$
($\eta=100$ ft.) AND λ IS AN EXPONENTIAL FUNCTION

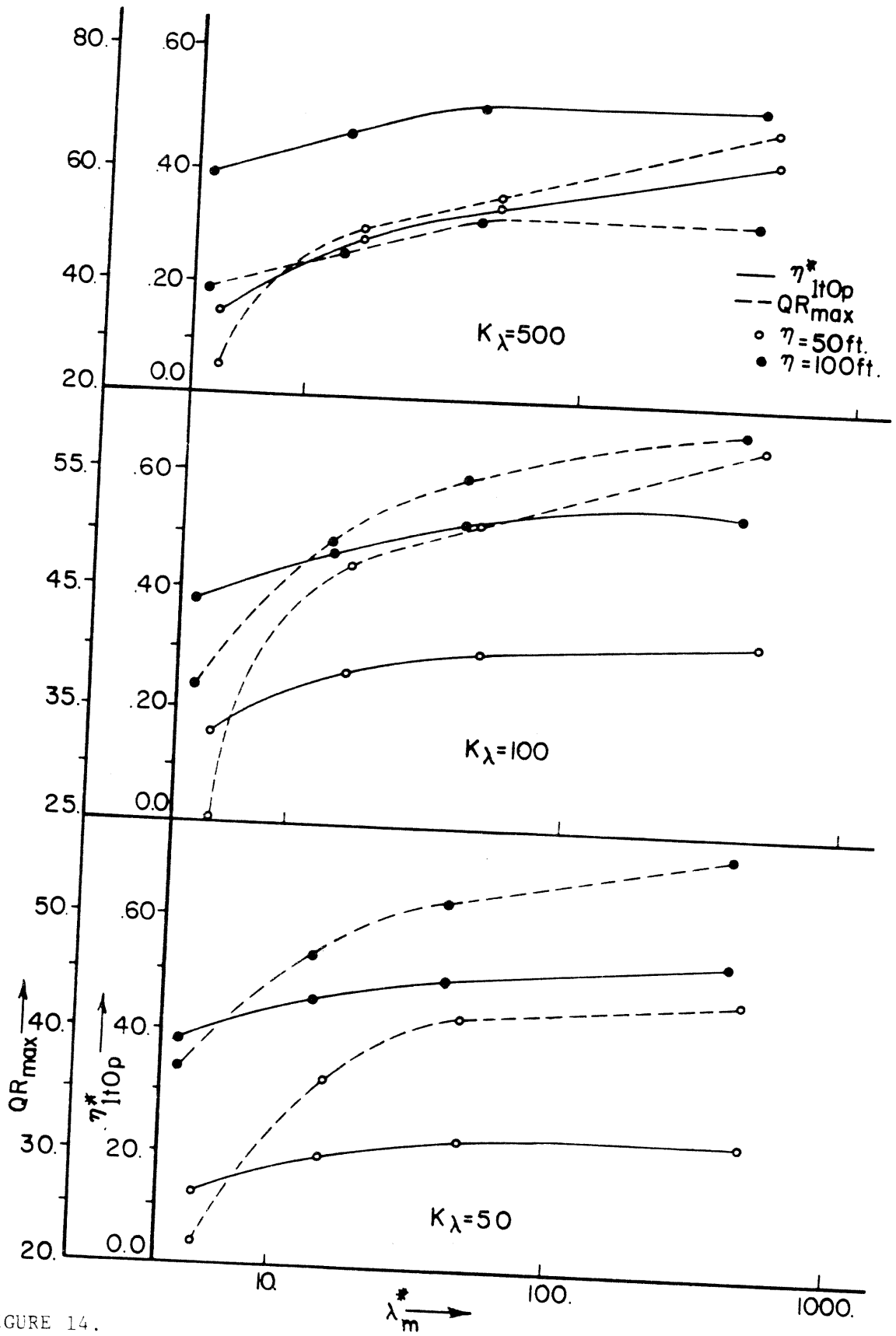


FIGURE 14.

assumed to be an exponential failure rate as described by Eq. 7. The prediction curves in Figs. 13 and 14 are similar to those in Figs. 7 and 8, respectively. The exponential failure rate produces values of η_{1t0p}^* and QR_{max} which are approximately 10% greater than those computed for a constant failure rate. In Figs. 13 and 14, QR_{max} assumes values in the range of 10 to 75%.

Sensitivity to Variations in Fixed Parameters. - The sensitivity of the η_{1t0p}^* and QR_{max} values, as presented in Fig. 8, to variations in the values of the "fixed parameters" is shown in Table 1. The variations in the values of the fixed parameters span the practical range of each. The sensitivity is determined as an average percentage change in the values of η_{1t0p}^* and QR_{max} as determined with the fixed parameters having the values designated in the preceding section.

Variations in K_1 , η_{sp}^* , z and n result in changes of about 10% or less in η_{1t0p}^* and QR_{max} . Variations in τ and C_v produce more significant changes in η_{1t0p}^* of approximately 12 to 30%. Also, as noted in Table 1, variations in τ and C_v produce changes in QR_{max} of approximately 15 to 38%. Variations in η_{ld}^* result in significant changes in η_{1t0p}^* and QR_{max} when $K_\lambda = 100$ and $\eta = 50$ ft; however, the changes are not significant when $K_\lambda = 500$ and $\eta = 50$ or 100 ft.

Computation Time. - The maximum computation time C_t in seconds, which is required for the numerical model to determine the transient hydraulics, for a particular set of geometric, hydraulic and dynamic parameters, may be approximated by the following

TABLE 1. SENSITIVITY OF η_{lt0p}^* AND QR_{max} TO VARIATIONS IN

K_1 , η_{ld}^* , η_{sp}^* , z , τ , C_v AND n FOR $L=10,000$ ft.,

$\tau=10$, $\lambda_c=0.01$ fps

Fixed Variable	Value	K_λ	Avg. Percentage Variation in η_{lt0p}^*		Avg. Percentage Variation in QR_{max}	
			$\eta=50$ ft.	$\eta=100$ ft.	$\eta=50$ ft.	$\eta=100$ ft.
			(4)	(5)	(6)	(7)
(1)	(2)	(3)				
K_1	1.1	100	-12.4	+ 9.1	+14.0	+ 8.5
	1.3	100	+ 1.3	+ 0.2	- 2.1	+ 8.3
	1.1	500	+ 1.9	+12.9	+10.0	+ 2.5
	1.3	500	+ 5.3	- 7.5	- 2.6	+ 2.3
η_{ld}^*	0.01	100	-28.8	- 1.9	-10.7	- 4.2
	0.05	100	+18.5	+ 8.0	+17.3	+17.3
	0.01	500	- 6.7	- 1.5	+ 1.8	+ 5.0
	0.05	500	+ 2.6	+ 0.9	+ 6.0	+15.6
η_{sp}^*	0.900	100	- 6.5	+ 0.5	+ 1.5	+ 4.2
	0.975	100	-14.0	+ 3.6	+14.5	+ 6.3
	0.900	500	+18.0	-10.5	+11.5	+ 3.4
	0.975	500	+ 2.7	+18.2	+ 2.9	+ 3.5
z	0.0	100	-11.5	- 5.4	- 5.8	+13.6
	4.0	100	- 5.8	+18.0	+ 1.6	+ 6.2
	0.0	500	- 1.2	- 2.8	- 7.2	+ 9.8
	4.0	500	+ 4.6	+ 0.5	+13.3	- 2.6
n	0.02	100	- 7.3	+ 1.8	+ 3.4	+ 6.1
	0.06	100	- 5.7	+ 1.9	+18.0	+ 2.4
	0.02	500	+ 1.0	+ 1.1	+ 4.1	+ 5.0
	0.06	500	+ 1.4	+ 4.0	+11.9	+ 5.3
τ	5.0	100	-20.0	-16.6	-17.0	+37.6
	5.0	500	+17.2	- 7.0	-14.4	+38.1
C_v	1.0	100	-25.5	-24.0	-37.3	+21.7
	1.0	500	5.5	-36.3	-12.2	+13.3

$$C_t \approx C_p + K_{op} C_{kt} T \dots \dots \dots (103)$$

$$\text{where } T = \frac{N}{2L\lambda_c} \left[\frac{Q_o}{\eta(c_1 - c_2)} + \sqrt{\frac{g\eta(c_1 - c_2)}{c_1}} \right] [\eta + \eta_{1d}(K_\lambda - 1)] \dots (104)$$

and C_p is the constant compile time, K_{op} is a multiplier which reflects the additional computation time required when the retarding layer optimization procedure is utilized, and C_{kt} is a constant. When the computations are performed on an IBM/360 computer, $C_p = 94$ seconds and $C_{kt} = 0.020$ seconds. If the retarding layer elevation is not optimized, $K_{op} = 1$; otherwise, K_{op} varies from 4 to 10 depending upon the magnitude of $(\eta_{1d}^* - \eta_{vmp}^*)$.

SUMMARY AND CONCLUSIONS

A conceptual method to reduce flood wave peaks due to over-topping failures of small homogeneous earthfill dams has been introduced. A numerical simulation model based upon a characteristic numerical solution of the St. Venant unsteady flow equations is presented for predicting the transient reservoir flow produced by the gradual breach of an earthfill dam.

The extent of reduction in the reservoir outflow from a breached dam due to the presence of a hypothetical erosion retarding layer is presented, along with the optimal elevation of the retarding layer, for a wide range of pertinent geometric, hydraulic, and dynamic parameters. The extent of reduction QR_{max} in the maximum outflow is primarily related directly to the ratio of the failure rate of the earthfill dam to the failure rate of the erosion retarding layer, i.e. K_λ , and to the dimensionless failure rate λ^* which is defined by Eq. 19. This

reduction can be as significant as 75%. The dimensionless optimal elevation η_{1tOp}^* , which minimizes the maximum reservoir outflow due to the breach, is related directly to the height η of the dam, K_λ , and λ^* and inversely to the length L of the prismatic reservoir and to the failure rate λ . The exponential failure rate produces values of η_{1tOp}^* and QR_{max} which are approximately 10% greater than those computed when the failure rate is constant.

Some sensitivity tests of the numerical model indicate that variations in the ratio of the width to the length of the prismatic reservoir, i.e. τ , and the coefficient of discharge C_v of the V-breach significantly effect the extent of reduction in outflow achieved by a retarding layer, as well as, its optimal elevation. Variations in the dimensionless thickness η_{ld}^* of the retarding layer produce some significant changes in η_{1tOp}^* and QR_{max} as η and K_λ assume smaller values. However, variations in the ratio of the total length L' of the reservoir to the length L of the prismatic portion of the reservoir, i.e. K_1 , the dimensionless elevation η_{sp}^* of the spillway crest, the side slope z of the trapezoidal reservoir cross section, and the Manning roughness coefficient n produce relatively small changes in η_{1tOp}^* and QR_{max} .

When the prismatic reservoir length is small, say $L=2000$ ft., the reservoir storage is depleted at a significantly increasing rate as the breach forms. Hence, for failure rates of 0.01 fps and smaller, the reservoir water surface may eventually recede at a rate which is faster than that at which the breach forms. Thus, the elevation of the tip of the V-breach may be in the vicinity of $\eta/2$ when the maximum outflow is attained. The optimal elevation of the retarding layer is located

above this; and its location is critical since an incorrect positioning can cause the outflow to exceed the maximum that would occur when no erosion retarding layer is present. When this condition exists and $\eta=100$ ft., the reduction in the maximum outflow is relatively small as compared to that achieved by a retarding layer in an earthfill dam of a reservoir with a larger surface area.

The numerical model, as presented herein, may be used in its present form or modified, as required, to investigate the transient hydraulics of prismatic reservoirs subjected to unsteady flow introduced at either or both extremities of the reservoir.

ACKNOWLEDGEMENTS

The work upon which this paper is based and was supported in part by funds provided under Project No. A-0-35-M0 of the United States Department of the Interior, Office of Water Resources Research, as authorized under the Water Resources Act of 1964, Dr. T. E. Harbaugh principal project investigator.

The writer would like to express special appreciation to Dr. T. E. Harbaugh of the Civil Engineering faculty, University of Missouri-Rolla for his advice concerning the research reported herein and for his extensive review of the paper.

APPENDIX I. - REFERENCES

1. Amein, Michael, and Ching S. Fang, "Implicit Flood Routing in Natural Channels," *Journal of the Hydraulics Division*, ASCE, Vol. 90, No. HY12, Proc. Paper 7773, December, 1970, pp. 2481-2500.
2. Amein, M., "Streamflow Routing on Computer by Characteristics," *Water Resources Research*, Vol. 2 (1), 1966, pp. 123-130.

3. Amein, M. and C.S. Fang, *Streamflow Routing (with application to North Carolina Rivers)*, Report No. 17, Water Resources Research Institute of the University of North Carolina, Raleigh, N.C., 1969.
4. Baltzer, Robert A. and Chintu Lai, "Computer Simulation of Unsteady Flow in Waterways," *Journal of the Hydraulics Division*, ASCE, Vol. 94, No. HY4, Proc. Paper 6048, July 1968, pp. 1083-1117.
5. Chow, Ven T., *Open-Channel Hydraulics*, McGraw-Hill Book Co., New York, 1959.
6. Conte, S.D., *Elementary Numerical Analysis*, McGraw-Hill Book Co., New York, 1965.
7. Dronkers, J.J., "Tidal Computations for Rivers, Coastal Areas, and Seas," *Journal of the Hydraulics Division*, ASCE, Vol. 95, No. HY1, Proc. Paper 6341, January, 1969, pp. 29-77.
8. Ellis, John, "Unsteady Flow in Channel of Variable Cross Section," *Journal of the Hydraulics Division*, ASCE, Vol. 96, No. HY10, Proc. Paper 7583, October, 1970, pp. 1927-1945.
9. Fletcher, F. Alan and Wallis S. Hamilton, "Flood Routing in an Irregular Channel," *Journal of the Engr. Mech. Division*, ASCE, Vol. 93, No. EM3, Proc. Paper 5287, June 1967, pp. 45-62.
10. Fread, D.L. and T.E. Harbaugh, "Gradually Varied Flow Profiles by Newton's Iteration Technique," *Journal of Hydrology*, Vol. 2, 1971, pp. 129-139.
11. Fread, D.L. and T.E. Harbaugh, *Numerical Simulation of Transient Open-Channel Flow*, Civil Engineering Department, University of Missouri-Rolla, Rolla, Missouri, January 1971.
12. Fread, D.L. and T.E. Harbaugh, "Simulation Program for the Transient Hydraulics Produced by Gradually Breached Earth Dams," *Hydraulic Series Bulletin*, Civil Engineering Studies, University of Missouri-Rolla, Rolla, Missouri, May 1971.
13. Garrison, Jack M., Jean-Pierre P. Granju, and James T. Price, "Unsteady Flow Simulation in Rivers and Reservoirs," *Journal of the Hydraulics Division*, ASCE, Vol. 95, No. HY5, Proc. Paper 6771, September, 1969, pp. 1559-1516.
14. Harbaugh, T.E., *Numerical Techniques for Spatially Varied Unsteady Flow*, Water Resources Research Center, University of Missouri, Report No. 3, 1967.
15. Henderson, F.M., *Open-Channel Flow*, Macmillan Co., New York, 1967.
16. Isaacson, E., J.J. Stoker and A. Troesch, "Numerical Solution of Flow Problems in Rivers," *Journal of the Hydraulics Division*, ASCE, Vol. 84, No. HY5, Proc. Paper 1810, October 1958, pp. 1810-1-1810-18.
17. Ligget, James A., "Mathematical Flow Determination in Open Channels," *Journal of Engr. Mech. Division*, ASCE, Vol. 94, No. EM4, Proc. Paper 6078, August 1968, pp. 947-963.
18. Ligget, J.A., and D.A. Woolhiser, "Difference Solutions of the Shallow-Water Equations," *Journal of the Engr. Mech. Division*, ASCE, No. EM2, April 1967, pp. 39-71.
19. Lister, Mary, "The Numerical Solution of Hyperbolic Partial Differential Equations by the Method of Characteristics," *Mathematical Methods For Digital Computers*, Edited by Anthony Ralston and Herbert S. Wilf, John Wiley & Sons, Inc., New York 1960.

20. Middlebrooks, T.A., "Earth-Dam Practice in the United States," *Centennial Transactions*, ASCE, Vol. CT, Paper No. 2620, 1953, pp. 697-722.
21. Morgali, James R., "Laminar and Turbulent Overland Flow Hydrographs," *Journal of the Hydraulics Division*, ASCE, Vol. 96, No. HY2, Proc. Paper 7069, February 1970, pp. 441-460.
22. Morgali, J.R. and R.K. Linsley, "Computer Analysis of Overland Flow," *Journal of the Hydraulics Division*, ASCE, Vol. 91, No. HY3, Proc. Paper 4325, May 1965, pp. 81-100.
23. Mozayeny, Bahram and Charles S. Song, "Propagation of Flood Waves in an Open Channel," *Journal of the Hydraulics Division*, ASCE, Vol. 95, No. HY3, Proc. Paper 6561, May 1969, pp. 877-892.
24. Smith, G.D., *Numerical Solution of Partial Differential Equations*, Oxford University Press, New York, 1965.
25. Strelkoff, Theodor, "The One-Dimensional Equations of Open-Channel Flow," *Journal of the Hydraulic Division*, ASCE, Vol. 95, No. HY3, Proc. Paper 6557, May 1969, pp. 861-876.
26. Strelkoff, Theodor, "Numerical Solution of Saint-Venant Equations," *Journal of the Hydraulics Division*, ASCE, Vol. 96, No. HY1, Proc. Paper 7043, January 1970, pp. 223-252.
27. Stoker, J.J., *Water Waves*, Interscience Publishers Inc., New York 1966.
28. Streeter, Victor L. and E. Benjamin Wylie, *Hydraulic Transients*, Chap. 15, McGraw-Hill Book Co., New York, 1967.
29. Terzidis, George, "Discontinuous Unsteady Flow in Open Channels," *Doctoral Dissertation*, University of California at Davis, 1968.
30. Terzidis, George and Theodor Strelkoff, "Computation of Open Channel Surges and Shocks," *Journal of the Hydraulics Division*, ASCE, Vol. 96, No. HY12, Proc. Paper 7780, December 1970, pp. 2581-2610.
31. Vineyard, Jerry D., "Pinkston Dam Failure," *Mineral Industry News*, Vol. 8, No. 6, June 1968, pp. 59-61.
32. Wylie, E.B., "Control of Transient Free-Surface Flow," *Journal of the Hydraulics Division*, ASCE, Vol. 95, No. HY1, Proc. Paper 6360, January 1969, pp. 347-361.
33. Wylie, E.B., "Unsteady Free-Surface Flow Computations," *Journal of the Hydraulics Division*, ASCE, Vol. 96, No. HY11, Proc. Paper 7683, November 1970, pp. 2241-2251.

APPENDIX II. - NOTATION

The following symbols are used in this paper:

A = Area of channel (reservoir) cross section

C_{kt}, C_p, C_t = Constants used in evaluating computation time, C_t ,
in Eq. 103

C_{sp}, C_v = Constants defined by Eqs. 94, and 93, respectively

C+, C- = Positive and Negative characteristics, respectively

- c_{sp}, c_v = Discharge coefficients for broad crested rectangular and V-shaped weirs, respectively
- c_1, c_2, c_3 = Constants defined by Eq. 12
- D = Hydraulic mean depth
- d, d_o, k, l, p, u, u_o = Subscripts denoting intersection points in the x^*-t^* plane
- F_d, F_g, F_u = Constants defined by Eqs. 96, 24 and 66, respectively
- $F_1, F_2, F_3, F_4, F_5, F_6$ = Constants defined by Eqs. 55-60, respectively
- G_1, G_2 = Constants defined by Eqs. 25 and 26, respectively
- g = Acceleration due to gravity
- I, II = Subscripts denoting location along an elementary channel
- K_{c1}, K_{c2} = Experimental constants
- K_e, K_1, K_s = Constants defined by Eqs. 8, 5 and 38 respectively
- K_{op} = Constant used in evaluating C_t
- K_λ = Ratio of the failure rate of earthfill dam to the failure rate of the erosion retarding layer
- $K_1, K_2, K_3, K_4, K_5, K_6$ = Constants defined by Eqs. 15-18, 91 and 92, respectively
- L = Length of prismatic section of reservoir
- L' = Length for determining S_o , and defined by Eq. 5
- L_{sp} = Length of emergency spillway crest
- N = Number of stations along reservoir
- n = Manning's roughness coefficient
- P = Wetted perimeter of flow cross section
- Q_o = Initial steady flowrate in reservoir
- Q_d = Flowrate at downstream boundary (reservoir outflow)
- Q_{dm} = Maximum flowrate at downstream boundary
- Q_{dmp} = Maximum possible flowrate at downstream boundary

- QR = Percentage reduction in Q_{dmp} and defined by Eq. 99
 QR_{max} = Maximum value of QR
 Q_t = Total outflow from experimental reservoir from time t_o to t_f , and defined by Eq. 102
 R = Hydraulic radius
 S_f = Friction slope (slope of energy gradient) defined by Eq. 3
 S_o = Bottom slope of reservoir and defined by Eq. 4
 T = Top width of free surface of channel (reservoir)
 t = Time
 t_o, t_f = Starting and ending times, respectively for experimental runs
 v = Average velocity in channel (reservoir)
 v_η = Average velocity at downstream boundary when $t = 0$
 x = Distance along channel (reservoir)
 x' = Unknown variable in Newton Iteration Technique
 y = Depth of flow in channel (reservoir)
 y_c = Critical depth for steady flowrate Q_o
 y_d = Depth of flow at downstream boundary
 y_n = Normal depth for steady flowrate Q_o
 y_s = Sequent depth of y_n
 z = Side slope of reservoir cross section
 δ = Very small increment
 δx = Increment of channel (reservoir) length
 $\delta \eta_{lt}^*$ = Incremental increase in η_{lt}^*
 η = Elevation of top of dam, with datum line at bottom of dam
 η_{lb} = Elevation of bottom of erosion retarding layer
 η_{ld} = Thickness of erosion retarding layer

- n_{lt} = Elevation of top of erosion retarding layer
 n_{ltOp} = Optimal elevation of top of erosion retarding layer
 n_{sp} = Elevation of emergency spillway crest
 n_v = Elevation of bottom of V-breach when $t=t_d$
 n_{vo} = Elevation of bottom of V-breach when $t=t_{do}$
 θ = Angle of inclination of channel bottom with the horizontal
 λ = Failure rate of dam (rate of formation of the V-breach)
 λ_c = Constant failure rate during a specified period of time or interval of elevation, n_v
 λ_m = Estimated maximum failure rate when $n_v = n_{vmp}$
 σ_{yd} = Percentage standard deviation of y_d
 σ_{Qt} = Percentage standard deviation of Q_t
 T = Parameter used in evaluating C_t and defined by Eq. 104
 τ = Ratio of initial top width T to reservoir length L
 ϕ = Acute central angle of V-breach.
 ψ = Linear multiplier
 $*$ = Superscript denoting a dimensionless variable

VITA

Danny Lee Fread was born on July 17, 1938, in Tuscola, Illinois. He received his primary and secondary education in Lovington, Illinois. He received his college education from Carthage College, Kenosha, Wisconsin and the Missouri School of Mines and Metallurgy, Rolla, Missouri. In May 1961, he received a Bachelor of Science degree in Civil Engineering from the Missouri School of Mines and Metallurgy, Rolla, Missouri.

In June 1961, he accepted a position with Texaco Inc. as an Assistant Design Engineer at the Lawrenceville refinery and remained with that firm until September 1967. During this period, he was advanced to the position of Senior Design Engineer and was registered as a Professional Engineer in the State of Illinois.

He enrolled in the Graduate School of the University of Missouri-Rolla in September 1967. He was the recipient of a National Defense Education Act Fellowship for the period of September 1967 to September 1970. He received a Master of Science degree in Civil Engineering from the University of Missouri-Rolla in May 1969. Since September 1970, he has served as co-investigator on a research project supported by the United States Department of Interior, Office of Water Resources Research. This project provided the information upon which this dissertation is based.